63-2-5

PHILCO CORPORATION — Western Development Laboratories

In reply cite: 614-3-139
RWB/SSB/rdr
14 February 1963

SUBJECT: Contract AF04(695)-113
Submittal of Technical Report WDL-TR1993
As a deliverable item

TO: Commander
Space Systems Division
Air Force Systems Command
United States Air Force
Air Force Unit Post Office
Los Angeles 45, California

ATTENTION: Technical Data Center

INFO COPIES: D. Cowart, CSD #3 (1 copy)
B. Byrd Jr., AFSSD/SSOCK (w/o enclosure)

REFERENCE: (a) Contract AF04(695)-113, Exhibit "A"
(b) Section IV, Paragraph 3.18 of AFBM Exhibit 58-1
(c) Part XVIII Schedule of Contract AF04(695)-113

In accordance with the requirements of references (a), (b), and (c) we are forwarding ten (10) copies of the following document:

Title	Number and Data
Doppler Propagation Study	WDL-TR1993 31 January 1963

PHILCO CORPORATION
Western Development

R. W. Boyd
Manager, Contracts Management

TECHNICAL DOCUMENTARY REPORT

WDL-TR1993

31 JANUARY 1963

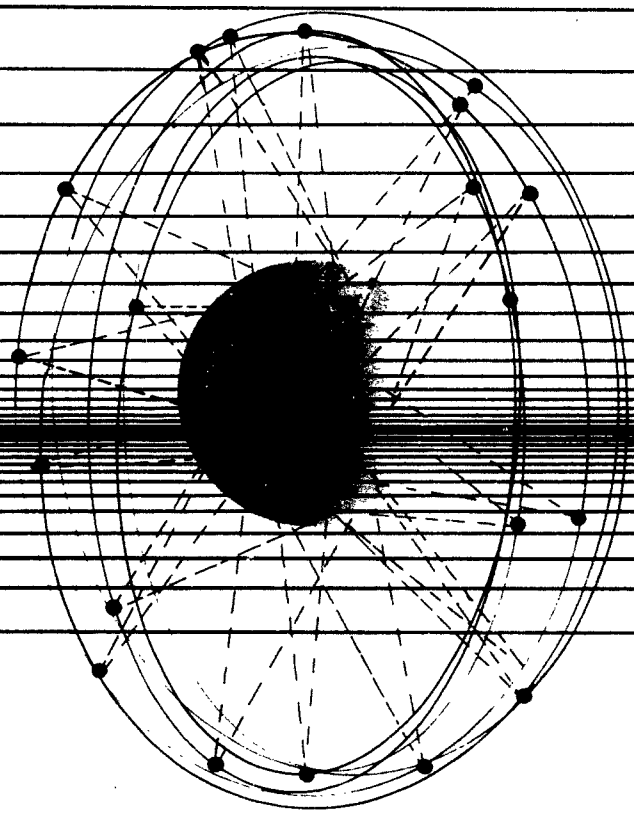

DOPPLER PROPAGATION STUDY

PREPARED FOR:

AIR FORCE SPACE SYSTEMS DIVISION
AIR FORCE SYSTEMS COMMAND
UNITED STATES AIR FORCE
INGLEWOOD, CALIFORNIA

AF04(695) -113

PHILCO
A SUBSIDIARY OF Ford Motor Company

WESTERN DEVELOPMENT LABORATORIES
PALO ALTO, CALIFORNIA

TECHNICAL DOCUMENTARY REPORT

DOPPLER PROPAGATION STUDY

Prepared by

PHILCO CORPORATION
Western Development Laboratories
Palo Alto, California

Contract No. AF04(695)-113

Prepared for

AIR FORCE SPACE SYSTEMS DIVISION
AIR FORCE SYSTEMS COMMAND
UNITED STATES AIR FORCE
Inglewood, California

ABSTRACT

PHILCO WDL-TR1993 UNCLASSIFIED
DOPPLER PROPAGATION STUDY pages
31 January 1963 Contract AF04(695)-113

This report describes Doppler propagation and the problems encountered in transmitting and receiving Doppler tracking signals through the atmosphere. It presents formulas for the Doppler shift, models of the atmosphere, and equations for atmospheric refraction. The information is combined in an analysis of Doppler errors caused by propagation effects and indicates the accuracies to be expected when dealing with Doppler shifts.

THIS UNCLASSIFIED ABSTRACT IS DESIGNED FOR RETENTION IN A STANDARD 3-BY-5 CARD-SIZE FILE, IF DESIRED. WHERE THE ABSTRACT COVERS MORE THAN ONE SIDE OF THE CARD, THE ENTIRE RECTANGLE MAY BE CUT OUT AND FOLDED AT THE DOTTED CENTER LINE. (IF THE ABSTRACT IS CLASSIFIED, HOWEVER, IT MUST NOT BE REMOVED FROM THE DOCUMENT IN WHICH IT IS INCLUDED.)

FOREWORD

This Technical Documentary Report on Definitive Contract AF04(695)-113 has been prepared in accordance with Exhibit A of that contract and Paragraph 3.18 of AFBM Exhibit 58-1, "Contractor Reports Exhibit," dated 1 October 1959, as revised and amended.

This report was prepared by Philco Western Development Laboratories in fulfilling the requirements of Part XVIII, Schedule of Contract AF04(695)-113.

TABLE OF CONTENTS

LIST OF ILLUSTRATIONS

SECTION 1

INTRODUCTION

In recent times, the Doppler effect has been used to measure the velocity of an aircraft or satellite with respect to an observer or tracking complex. The purpose of a tracking complex is to characterize the trajectory of a vehicle to such an accuracy that reliable predictions of its past and future positions can be made. The reliability of a particular prediction depends upon the following factors:

a. The uncertainty associated with the satellite's position and velocity vector during the time period immediately preceding prediction.

b. The accuracy of the mathematical model representing the satellite's physical environment.

It is the purpose of this report to discuss these problems with respect to the Doppler system. The Doppler system itself is described, and equations are developed for the Doppler shift. The uncertainty in vehicle position is developed following a discussion of the mathematical model representing the satellite's physical environment (atmospheric characteristics and related refraction effects).

SECTION 2

DOPPLER EFFECTS

2.1 GENERAL DOPPLER EFFECTS

The Doppler* effect is observed when a source of radiation is in motion with respect to an observer. It is characterized by an apparent change in the frequency of the emitted radiation. Assuming that the observer either knows or has a method of monitoring the original transmitted frequency of the radiation, the relative motion of the radiating source with respect to the observer can be determined. When the radiating source and the observer are moving toward each other, the observer notes a "shift" to a higher frequency caused by the "foreshortening" of the radiated wavelength. When the source and observer are moving away from each other, a decrease in frequency is noted, caused by the "lengthening" of the radiated wavelength. The amount of frequency or wavelength shift corresponds to the relative velocity of the source, whereas the increase or decrease in observed frequency or wavelength corresponds to the relative direction of movement of the source.

Doppler data systems, for example, extract frequency shift information and resolve it into relative velocity measurements. An angle generating system is frequently coupled with a Doppler data system to provide coordinated angles and range rates for the purposes of orbital operations and ephemeric constructions.

2.2 ONE-WAY DOPPLER SHIFT

Suppose a satellite moving with a velocity of magnitude V carries a radio transmitter operating at a frequency f_o. The Doppler frequency shift, f_d, is the difference between transmitted frequency, f_o, and received frequency, f_r, at an observation point:

$$f_d = f_o - f_r.$$

---

* Named for C. J. Doppler, physicist and mathematician, who first used this effect in 1842 in determining relative velocities of stars.

This Doppler shift may also be measured as the time rate of change of the phase difference between transmitted and received signals. The phase difference, $\emptyset$, is represented by:

$$\emptyset = f_o \, S/C$$

where c is the speed of light in a vacuum and S is the geometric path length between transmitter and receiver. The optical path length, S', may be expressed as an integral involving the refractive index:

$$S' = \int_0^S n(s)ds.$$

It has been found (Ref. 6) that the following inequalities hold between the distances D, S, and S':

$$D < S < S'$$

$$S - D < S' - S$$

where D is defined as the geometric length of a straight line from transmitter to receiver.

It is important to recognize that the refraction error in range, ΔR, is S' -D, not S - D. The difference between S and D is usually negligible, as can be seen by approximating the curved path between transmitter and receiver by a circular arc spanning chord D and subtending a central angle of ΔE. The angle ΔE is the "refractive error" in the apparent elevation angle E_o of the satellite. This yields the result

$$\frac{S - D}{S} \approx \frac{1}{6} (\Delta E)^2 \leqslant 10^{-5} \text{ or } 10^{-6}$$

for most elevation angles of practical use, or a maximum range error on the order of feet at ranges within which significant refraction errors will occur. The phase difference then becomes

$$\theta = \frac{f_o}{c} \int_0^S n(s)ds. \tag{2-1}$$

To get the time rate of change of the phase difference, the above expression is operated on by the Leibnitz rule for differentiating an integral involving a parameter:

$$\frac{d}{dt}\left[\frac{f_o}{c}\int_0^S n(s)ds\right] = \frac{f_o}{c}\left[n_t \frac{ds}{dt} + \int_0^S \frac{dn}{dt}\, ds\right]$$

$$= f_d \text{ (Doppler Shift)} \tag{2-2}$$

where n_t is the local index of refraction at the transmitter corresponding to the frequency f_o. The first term may be expanded to show the results of three effects. The first is the actual Doppler frequency. The second is an error term due to refractive bending of the wave path. Such bending results in a direction of arrival of the signal at the vehicle different from the straight line path from the ground to the vehicle. This causes the measured Doppler velocity to differ from the actual Doppler velocity. The third effect in the expanded first term in equation (2-2) is an error arising from the fact that the phase velocity of the wave at the vehicle is not equal to the speed of light.

The last term in equation (2-2) is a combination of two types of errors. One part of the term takes into account the error due to a change in the propagation path as the vehicle moves through different strata at a constant radio distance from the ground station. The other error arises from irregularities in the layers, such as rain, clouds, ion concentrations, etc. Usually the second term in equation (2-2) is

not considered or measured separately, with the result that it appears as a "noise" or "scintillation" effect riding on the first term. Generally, it is neglected* and equation (2-2) reduces to

$$f_d = \frac{f_o}{c} n_t \frac{ds}{dt} .$$

A general formula for the Doppler shift in one-way transmission may therefore be written:

$$f_d = f_o - f_r = \frac{f_o}{c} n_t \frac{ds}{dt}$$

or alternately,

$$f_r = f_o \left(1 - \frac{1}{c} n_t \frac{ds}{dt}\right). \qquad (2\text{-}3)$$

A sample graph of one-way Doppler shift, slant range, and elevation angle as a function of time for a typical satellite pass is presented in Fig. 2-1. The calculation for this graph assumed a spherical earth, a transmitted frequency of 400 Mc, and a vehicle altitude of 160 n.m.

2.3 TWO-WAY DOPPLER SHIFT

Consider a case where the signal is transmitted from the ground station, received in the satellite, and retransmitted to the ground station. If f_o is the frequency transmitted from the station and n_s is the index of refraction at the station corresponding to f_o, then the frequency received at the satellite is

$$f_r = f_o \left(1 - \frac{1}{c} n_s \frac{ds}{dt}\right).$$

* This is justified statistically. A discussion of the subject is given in Ref. 11.

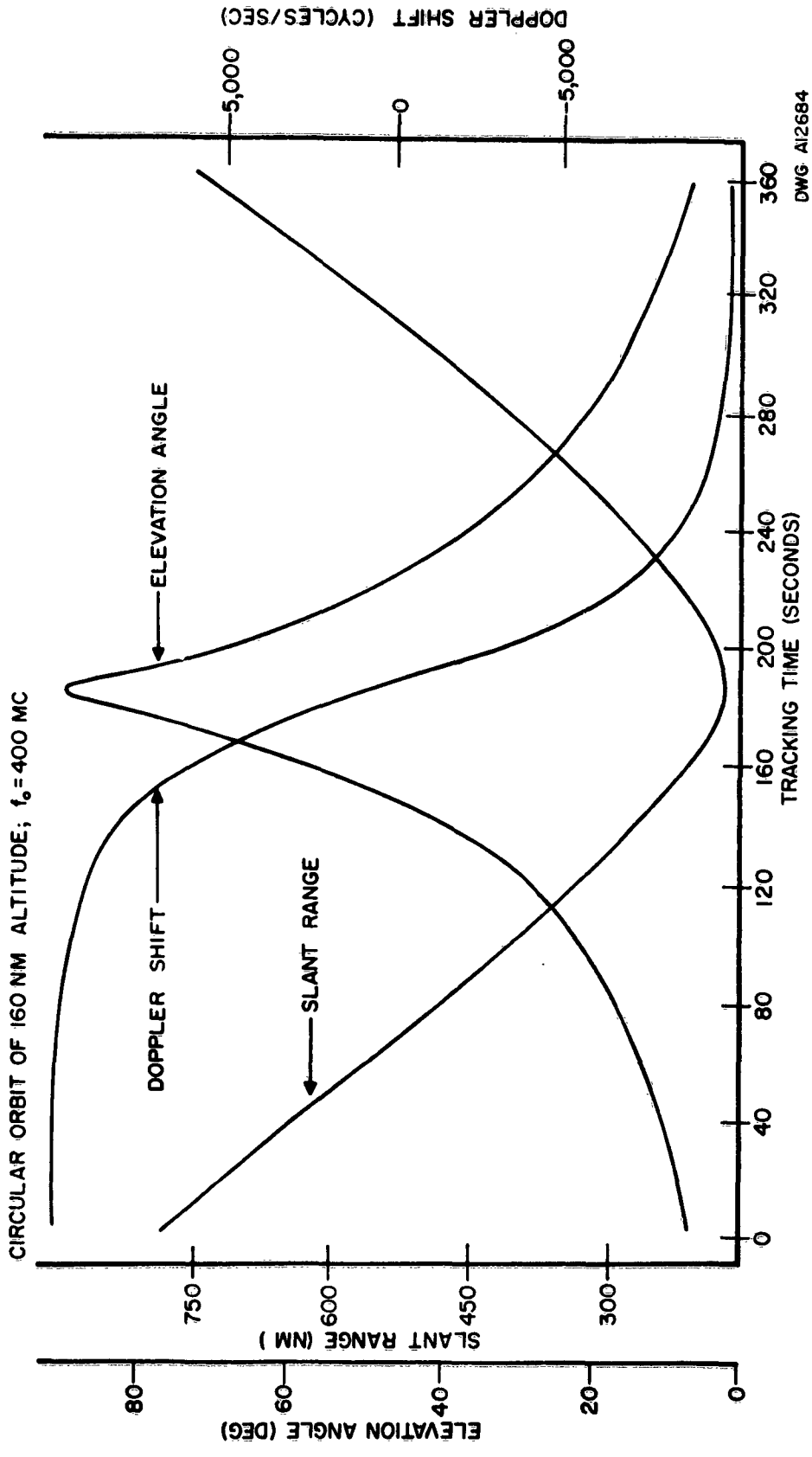

Fig. 2-1 One-Way Doppler Shift, Slant Range, and Elevation Angle

The transformed frequency in the satellite is

$$f_t = a + bf_r = a + bf_o \left(1 - \frac{1}{c} n_s \frac{ds}{dt}\right) \tag{2-4}$$

where a and b are known constants which depend upon the equipment in the satellite. (For example, a = 0 and b = 1 in the special case of skin tracking.) If n_t is the index of refraction at the satellite corresponding to f_t, then the frequency f_g received at the ground station is

$$f_g = f_t \left(1 - \frac{1}{c} n_t \frac{ds}{dt}\right). \tag{2-5}$$

The composite Doppler shift is found by combining equations (2-4) and (2-5):

$$\begin{aligned} f_d &= f_o - f_g = f_o - f_t \left(1 - \frac{1}{c} n_t \frac{ds}{dt}\right) \\ &= f_o - \left[a + bf_o \left(1 - \frac{1}{c} n_s \frac{ds}{dt}\right)\right]\left(1 - \frac{1}{c} n_t \frac{ds}{dt}\right) \\ &= f_o (1 - b) - a + \frac{1}{c} \frac{ds}{dt} \left[(a + bf_o)n_t + bf_o n_s\right] \\ &\qquad - bf_o n_s n_t \left(\frac{1}{c} \frac{ds}{dt}\right)^2. \end{aligned}$$

Neglecting the last term because of the smallness of $\left(\frac{1}{c} \frac{ds}{dt}\right)^2$, this becomes

$$f_d = f_o (1 - b) - a + \frac{1}{c} \frac{ds}{dt} \left[(a + bf_o)n_t + bf_o n_s\right]. \tag{2-6}$$

In the case of skin tracking (a = 0, b = 1),

$$f_d = f_o \frac{1}{c} \frac{ds}{dt} (n_s + n_t). \tag{2-7}$$

As previously mentioned, the general formulas which have been used here are affected by refractive bending. In order to determine the effect of this on accuracy, the next several sections will deal with the refraction errors in elevation angle and the mathematical model of the satellite's physical environment, the atmosphere. The equation for refractive bending will be derived and applied to correct the Doppler measurements.

SECTION 3

ATMOSPHERIC CHARACTERISTICS

3.1 GENERAL

As a radio wave passes between the satellite and the ground, it is affected by the medium through which it travels. The propagation medium will attenuate, reflect, and refract the wave. At the frequencies under consideration for tracking, attenuation and reflection by the propagating medium are of a negligible magnitude; but the effect of refraction normally may not be ignored.

Atmospheric refraction deteriorates the accuracy of Doppler measurements. To some extent, the refractive effects can be predicted and the tracking data can be corrected. As the various portions of the wavefront encounter atmospheric regions of differing refractive indexes, their velocities will be increased or decreased so that the net effect is a bending of the ray path toward the perpendicular in regions of higher index and away from the perpendicular in regions of lower index. Various methods for compensating refractive errors have been devised, but it is obvious that a complete correction requires a continuous profile of refractive index along the signal path.

3.2 INDEX OF REFRACTION

The index of refraction, n, for electromagnetic radiation at a given point in the atmosphere is defined as the ratio of the speed of radiation in a vacuum to the speed of radiation at the given point. Since the atmospheric index may differ from unity by several hundred parts per million, another parameter called the "refractivity" is often used. This parameter, N, is numerically more convenient and is defined as follows:

$$N = (n - 1)\ 10^6.$$

3.3 SPHERICALLY STRATIFIED ATMOSPHERE

As a first approximation, the shape of the earth is considered spherical. In the atmosphere surrounding this sphere, the mean density of the gas decreases approximately exponentially with increasing altitude. Usually under relatively quiet atmospheric conditions, the vertical gradient of refractivity is much greater than the horizontal gradient. (In fact, it is felt that the azimuthal or horizontal errors in Ref. 11 are less than 10 percent of the magnitude of the elevation or vertical errors.) For such reasons, but principally for mathematical simplicity, it is customary to assume that the refractivity is solely a function of altitude or of distance from the center of the earth. However, it is understood that such a spherical model deviates from the actual conditions in at least two ways. Because of diurnal, meteorological, and seasonal fluctuations of atmospheric conditions, the refractivity profile varies considerably with geographic location. In some cases, the solar zenith angle (i.e., local time and geographic position) also becomes an important factor (Appendix A of Ref. 3). Further, the figure of the earth is ellipsoidal rather than spherical.

The principal differences between refraction in the concentric spherical atmospheric stratification and in the confocal ellipsoidal stratification may be noted as follows. The angular refraction in the zenith direction is zero in the spherical model, but generally non-zero in the ellipsoidal case. In a spherical model, the ray path is a plane curve and its angle of arrival at the station is independent of the azimuth of the ground projection of the ray. In the ellipsoidal stratification, the ray path is a space (nonplanar) curve and its angle of arrival at the station depends upon the azimuth of the ground projection of the ray. For instance, considering rays which make equal 45° angles with a normal to the earth-spheroid at infinity, the ones reaching the station from the east or west will arrive at an elevation angle slightly greater (about 2 seconds of arc at a station on the equator) than that of such rays arriving from north or south. Considering rays which are inclined at 45° to the polar and to the equatorial

radii at infinity, the elevation angle of arrival at the equator may be some 11 minutes of arc greater than the corresponding angle at the pole due to the difference in earth-curvature alone. Such conclusions depend upon ellipsoidal geometry and the nature of the equations for refraction in the concentric spherical stratification. By differentiating these equations, it may be shown that the local mean radius of earth-curvature need be known only with an accuracy comparable to the inherent angular accuracy of the tracking system when approximating the ellipsoidal stratification by a spherical stratification. Since the inherent angular accuracy is on the order of one part in 10^5 in the most accurate present systems, this figure represents the approximate maximum accuracy for specifying the mean radius of earth curvature at a tracking station.

Because of the small eccentricity (0.082) of the earth spheroid, the maximum difference in the principal radius of curvature at the station is about one part in 10^5. Hence, in making refraction corrections, the model of a spherically-stratified atmosphere is sufficient for all existing tracking systems, provided the local mean radius of earth curvature is determined with an accuracy of one part in 10^{5*}. The current accuracy in the radius is close to this value.

In considering the spherical stratification of the earth's atmosphere, certain layers distinguish themselves one from the other, especially with regard to index of refraction. For example, the lower level (troposphere) has a positive refractivity and the upper level (ionosphere) has a negative refractivity.

---

* In computing the mean radius at a station, the geodetic latitude must be known to $\pm$ 5 minutes of arc. The mean radius is

$$R_e = b/(1 - e^2 \sin^2\phi)$$

where ϕ = geodetic latitude of the station,
e = eccentricity of the earth model, and
b = semi-minor axis (polar radius).

3.4 TROPOSPHERE

The troposphere is that portion of the atmosphere below about 40 nautical miles in which clouds form, convective disturbances occur, and temperature decreases with altitude. In the troposphere, the refractivity is a function of meteorological variables such as water vapor pressure, air temperature, and air pressure although independent of radio frequency up to 30 kMc. The refractivity is approximated by

$$N = (n - 1)\ 10^6 = \frac{a}{T}\left(P + \frac{be}{T}\right)$$

where N = refractivity,

n = index of refraction,

T = temperature in degrees Kelvin,

P = air pressure in millibars,

e = water vapor pressure in millibars,

a = constant, 77.6° K/mb, and

b = constant, 4810° K.

Since it is not usually convenient to determine the pressure and temperature at an arbitrary point in space, models are employed to represent the troposphere. Experimental evidence has substantiated that in the troposphere the mean refractive index decreases approximately exponentially with increasing altitude, while also varying with geographic location. The CRPL Exponential Radio Refractivity Atmosphere or "exponential reference atmosphere" is a good single-function representation of refractivity for the troposphere. The model calculates the refractivity as a function of general altitude, h; the altitude of the station, h_s; and the refractivity at sea level at the point in question, N(0).

The CRPL Exponential Radio Refractivity Atmosphere is presented (Ref. 3) in the following form:

$$N(h) = N(h_s) \exp\left[-P_e (h - h_s)\right] \qquad (3\text{-}1)$$

$$P_e = \log_e \left[N(h_s)/N(1)\right]$$

$$N(h_s) = N(0) \exp(-0.1958\, h_s)$$

$$N(1) = N(0) \exp(-0.1958)$$

where h = any desired height (n.m.) above mean sea level,
h_s = height (n.m.) of station above mean sea level,
$N(h_s)$ = refractivity at altitude h, and
$N(0)$ = sea level refractivity corresponding to $N(h_s)$*.

The exponential reference atmosphere is presented in Fig. 3-1 for the special case of a station at sea level.

The mean refractive index is significantly affected by such variables as season of the year, time of day, and instantaneous weather conditions (cold front, warm front, etc.). Although the theoretical tropospheric refractivity decreases exponentially with increasing altitude, an experimentally measured graph or "profile" of N versus altitude is therefore not a smooth curve. However, the primary refraction correction process mathematically depends upon the evaluation of integrals whose integrand is a function of the refractivity. Since integration is a smoothing process, the irregularities in the refractivity profile tend to cancel each other; and the results are not very different from those obtained by the use of the approximate profile.

Altitude changes in the refractive index, such as those exhibited in Fig. 3-1, produce range and range rate errors by creating changes in the velocity of the wave. In the troposphere, the velocity is always

---

* $N(h_s)$ can be estimated from world charts (Ref. 2).

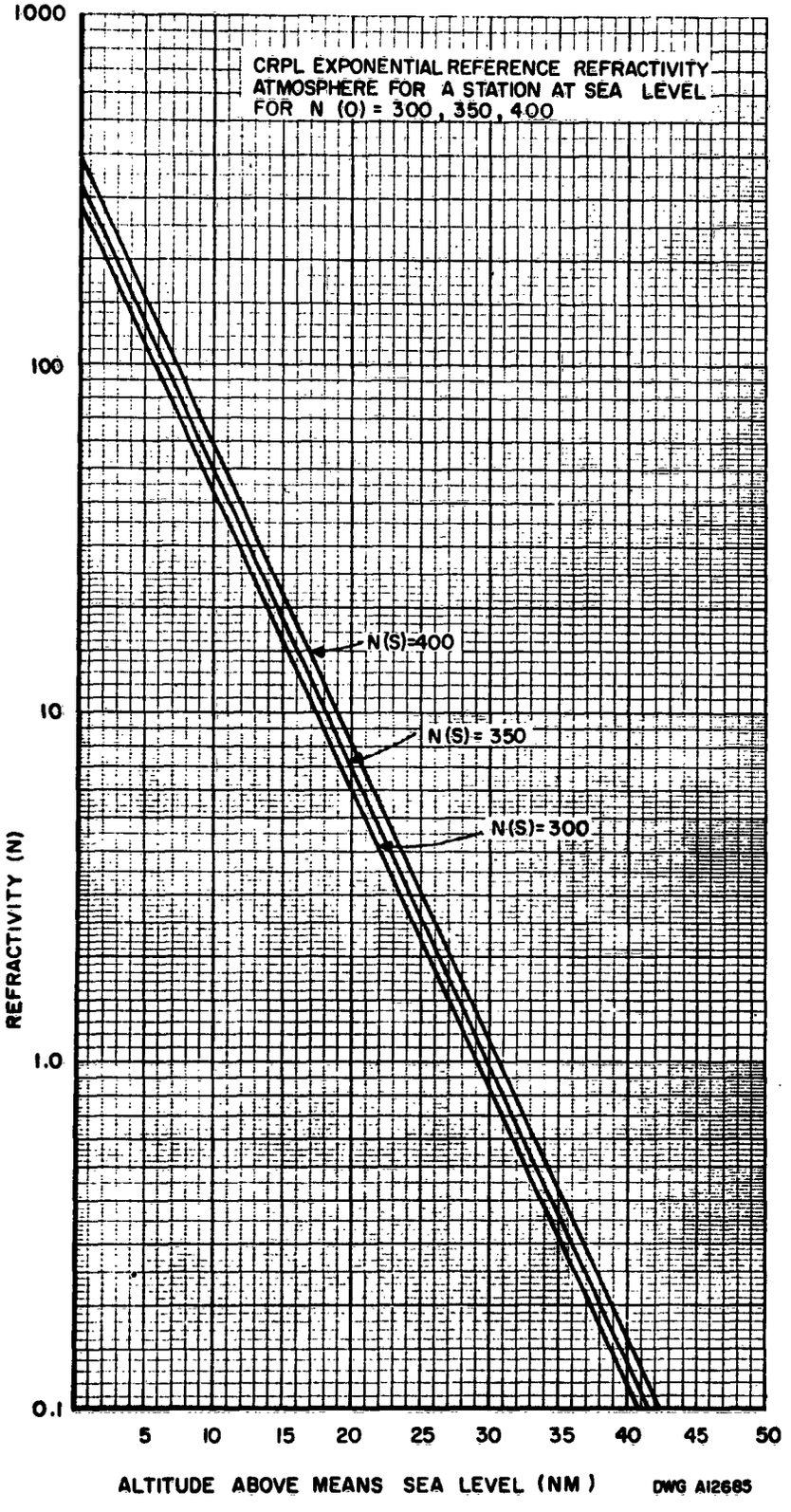

Fig. 3-1 CRPL Standard Model for Troposphere

less than the free space velocity which results in a time delay of the signal. In addition, the increased path length due to refraction further increases the apparent range. The range error due to the troposphere is independent of frequency, and variations of the state of the troposphere will cause the range error to fluctuate about a mean value. The percentage error due to tropospheric refraction is the same for range as for range rate (Doppler frequency).

3.5 IONOSPHERE

The ionosphere differs from the troposphere in that it contains a much higher number of positive and negative ions, which are produced by the ultraviolet and particle radiations from the sun. The increased ionization decreases the effective refractivity. The rotation of the earth on its axis, the annual course of the earth around the sun, and the development of sun spots all affect the number of ions present in the ionosphere; and these in turn affect the quality and distance of signal transmission.

Because of the variability of the ionosphere, it is difficult to make exact statements about the size of the tracking error. For example, at an altitude of 155 n.m., the ionospheric density has been found to vary as much as 100 percent daily. Throughout a sunspot cycle, the ion density has varied as much as 1600 percent (Ref. 3).

Different densities of ionization at different heights make the ionosphere appear to have layers. The D-layer lies between heights of 40 and 50 n.m. during the daytime. It is characterized by low ionization and an appreciable absorption effect. The E-layer is between 50 and 90 n.m. with the greatest density at 70 n.m. and the strongest effect in daylight hours. From 90 n.m. upward is the F-layer or layers: one layer at night and two layers (F_1 and F_2) during the daytime. The F-layer has the highest ionization and, therefore, the greatest effect on the refractivity.

Unlike the tropospheric case, the effect of refraction in the ionosphere is frequency dependent. Both the angle and range (range rate) deviations vary almost inversely with the square of the frequency. Ionospheric refractivity is a function of electron density and radio frequency. The ionospheric refractive index in an ionized gas (ignoring absorption) follows the following relationship:

$$n = \sqrt{1 - \left(\frac{f_c}{f_o}\right)^2} \qquad (3\text{-}2)$$

where f_o = signal frequency, and
f_c = plasma frequency or critical frequency.

The plasma frequency, f_c, is a term frequently used to express the function of elections and electron density in determining the index of refraction. The actual relationship is given as

$$f_c = \sqrt{\frac{N_e e^2}{m\pi}} \qquad (3\text{-}3)$$

where N_e = electron density,
e = electron charge, and
m = electron mass.

Substituting values for e, m, and π in equation (3-3) and combining with equation (3-2), the following formula is obtained:

$$n = \sqrt{1 - 80.5 \frac{N_e}{f_o^2}} \; . \qquad (3\text{-}4)$$

The electron density, N_e, must be known in order to calculate the refractive index by equation (3-4). Electron density profiles, giving N_e for various altitudes and geographic locations, can be obtained by ionosphere soundings; that is, actual measurements via rockets or probes.

In the absence of measured electron density profiles, the Chapman formula may be used as a model for the electron density in the ionosphere. The Chapman formula is the following:

$$N_e = N_m \exp \frac{1}{2} (1 - Z - e^Z \sec \zeta)$$

$$Z = \frac{h - h_m}{H}$$

$$H = \frac{kT}{mg}$$

where N_m = maximum electron density when the sun is overhead,

ζ = solar zenith angle,

h = any desired height in nautical miles above mean sea level,

h_m = height of maximum density N_m,

k = Boltzman's constant,

T = absolute temperature (at altitude h),

m = molecular mass of the gas, and

g = gravitational constant.

The average variations of the critical frequencies of the ionospheric layers are sufficiently well known to permit long-range predictions (accurate to within about 25 percent) of average conditions expected on "quiet" days. Such predictions are published three months in advance by the National Bureau of Standards. However, corresponding values of h_m and H must be known to obtain an electron density profile even when using the Chapman formula. Table 3-1 indicates the values of the parameters in Chapman's formula obtained from extensive pulse soundings and statistical analyses during periods between 1948 and 1954 at Washington D. C. (Ref. 4,5). Figure 3-2 shows some ionospheric electron-density profiles computed from Chapman's theory. The three solid curves represent the 2.5, 50.0, and 97.5 percent confidence limits of the statistical analysis. The broken curves are the noon and midnight results of a single experiment measuring refractivity. The

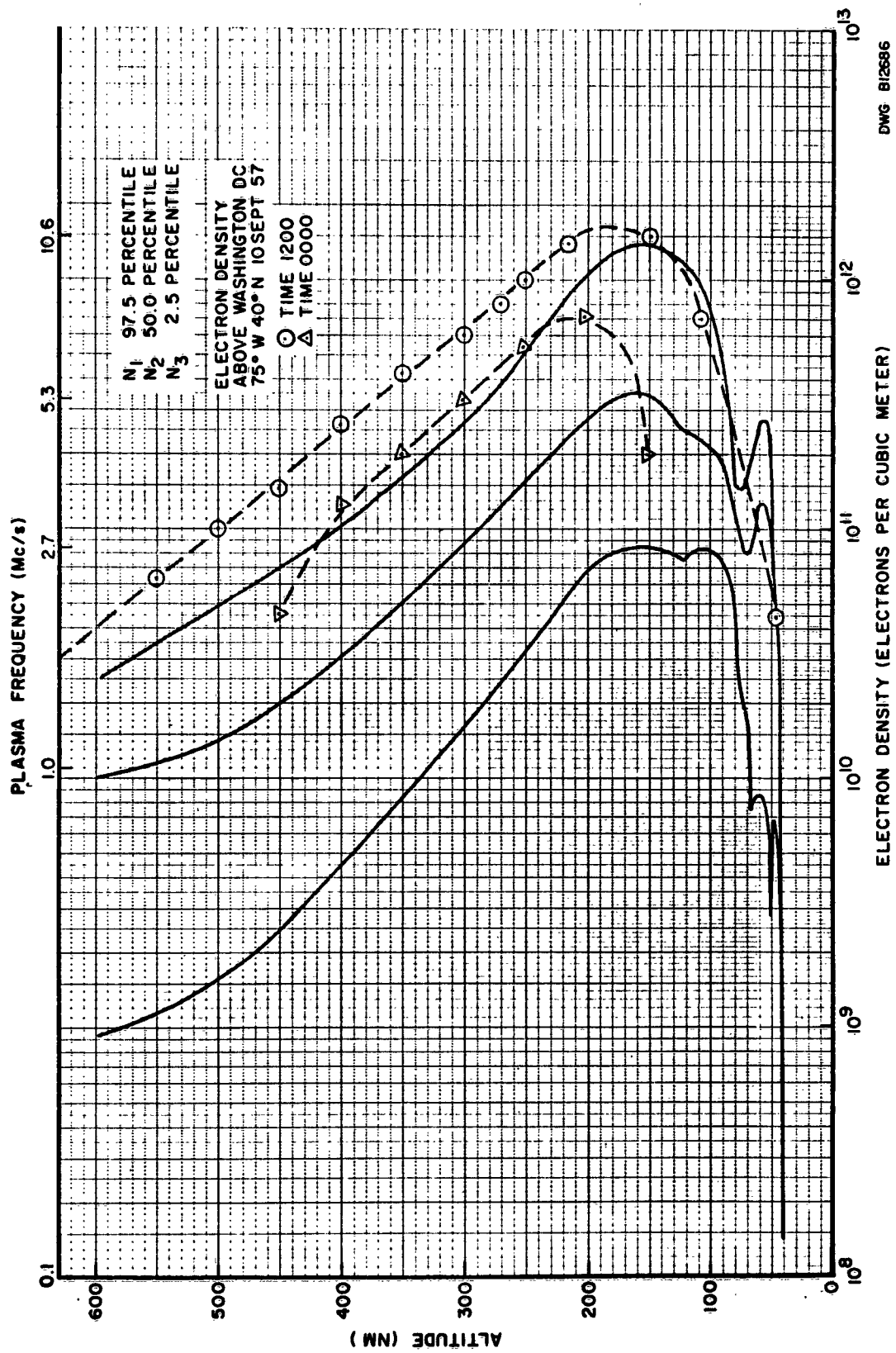

Fig. 3-2 Ionospheric Electron Density Profiles

critical (plasma) frequency corresponding to any point on a curve may be read on the upper horizontal scale, while the lower horizontal scale represents the electron density corresponding to each critical frequency. Figure 3-3 was obtained by using the information from Fig. 3-2 in equation (3-4) to obtain a refractivity profile for an operating frequency of 400 Mc.

TABLE 3-1

MAJOR CHARACTERISTICS OF IONOSPHERIC LAYERS

Layer	h_m average height (n. miles)	H scale height (n. miles)	Critical frequency and Maximum electron density*		
			2.5 percentile	rms or average	97.5 percentile
D	46	2.4	0.7	1.1	1.3
			6.0	15	20
E	58	5.9	0.9	3.3	4.8
			9.2	134	290
F_1	100	16	2.7	4.4	5.0
			90	240	310
F_2	150	38	2.7	5.3	10.6
			90	354	1400

* Upper value is critical frequency in megacycles per second; lower value is maximum electron density in units of 10^9 per cubic meter.

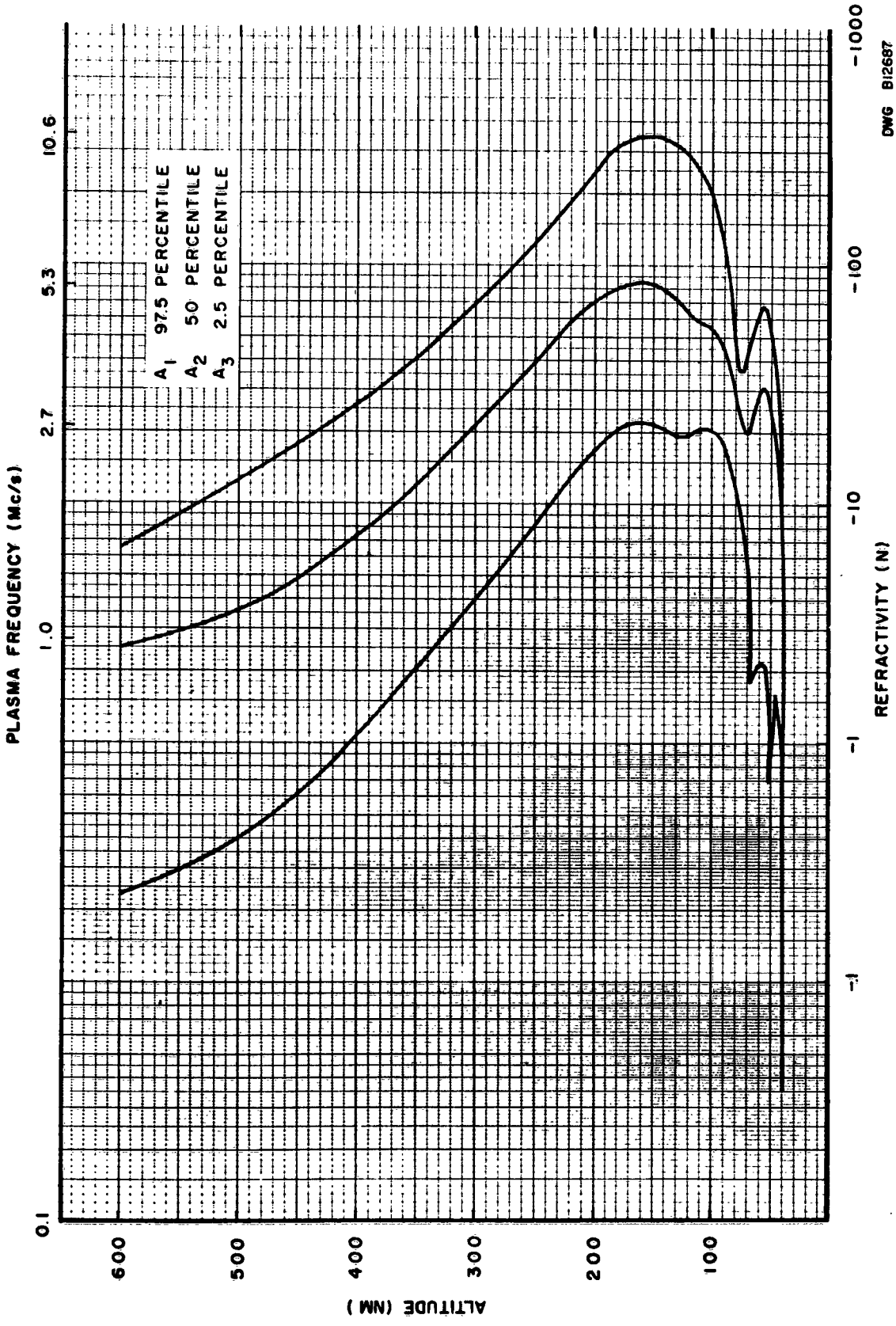

Fig. 3-3 Ionospheric Refractivity Profiles

3.6 STANDARD CORRECTIONS

Corrections for tropospheric angle refraction can be made in several ways. One method, based on the surface index of refraction, claims prediction accuracies of 0.02 milliradian at a 5-degree antenna elevation angle. A simpler model, using the yearly average of the station surface index of refraction, also reduced the refraction error significantly. Correction techniques using the world-wide, all-year average are also capable of reducing the error, although not as much as the above methods. The most practical correction method for use in tracking vehicles seems to be the yearly average of the station surface index of refraction.

Compensation for ionospheric effects can be carried out by methods similar to those used for tropospheric effects. By employing frequent ionospheric soundings to determine the profile of the ionosphere, the amount of expected refraction can be calculated. A less accurate method would be to use typical profiles either from past soundings at the station or from other stations near the same latitude. If this type of correction is used, a day profile and a night profile are needed. Using frequent soundings, the range rate and angle error can be reduced by as much as 80 percent. Since the ionization of the ionosphere can vary over such wide ranges, a correction made from average profiles does not seem to be very reliable.

Both the CRPL model for the troposphere and the Chapman model for the ionosphere are attempts to establish a "standard" atmosphere, although no such thing exits. Not only are there changes from day to day, but there are also turbulence layers as well as occasional clouds and precipitation particles. The use of a standard atmosphere model does not give perfect results; however, continuing investigations are yielding improved solutions to the problem.

SECTION 4

REFRACTION

4.1 GENERAL

The purpose for developing such models as the CRPL Exponential Atmosphere and the Chapman formula for electron density in the ionosphere is to enable a reconstruction of the signal path by the laws of refraction. Refraction correction formulas for optical or radio tracking instrumentation are generally based on the use of geometrical optics in a spherically-stratified terrestrial atmosphere.

4.2 GEOMETRICAL OPTICS

Geometrical optics is the limiting case of physical optics (based on Maxwell's electromagnetic wave equation) as the wavelength approaches zero, and its use is valid in ray tracking problems where the refractive index does not vary much in a distance comparable to the wavelength. The radio wavelength is about 10 feet at 100 Mc and about 1 foot at 1,000 Mc, while the atmospheric index at these frequencies normally changes only by amounts on the order of parts, or tenths of parts, per million over such distances. Hence, the use of geometrical optics in tracking problems appears well founded.

At the interface of two optical media with differing indexes of refraction, n_1 and n_2, the direction of a straight-line ray path will change. The incident ray, the line normal to the interface, and the refracted ray are all coplanar; if θ_1 and θ_2 are the angles between the normal and the two rays, then Snell's Law states that

$$n_1 \sin \theta_1 = n_2 \sin \theta_2$$

If a refractive medium has an index of refraction, n, which depends only on the distance, r, from a given point (spherical symmetry), then Bouguer's Law states that the ray path is described by

$$n_r \sin \phi = \text{constant}$$

where n and r pertain to any point on the ray and ϕ denotes the angle between the radius vector and the tangent to the ray path at the given point (ϕ is the complement of angle E_T in Fig. 4-1).

4.3 REFRACTION GEOMETRY

Figure 4-1 shows the typical spherical-earth, ray refraction geometry in the plane determined by the center of the earth O, a ground station S, and the ray path $\widehat{ST}$.

Let
- R = mean radius of the earth,
- h_s = height of station above mean sea level,
- h_t = height of target above mean sea level,
- Q_1TQ_2 = line tangent to the ray at T,
- SQ_3 = line tangent to the ray at S,
- STQ_4 = straight line through S and T (radial line),
- E_o = observed elevation angle,
- E = true elevation angle,
- ΔE = elevation angle error, $\Delta E = E_o - E > 0$,
- E_T = declination angle as observed from satellite,
- $E_T+\Delta E_T$ = declination angle as observed from station,
- ΔE_T = declination angle error,
- γ = total bending angle, $\gamma = \Delta E_T + \Delta E$,
- $N(h_s)$ = refractivity at the ground station,
- $N(h_t)$ = refractivity at the target, and
- $N(h_k)$ = refractivity at an altitude h_k above mean sea level.

If the refractivity profile for the function N(h) is not known exactly, it may be approximated by a standard atmosphere as in Section 3.

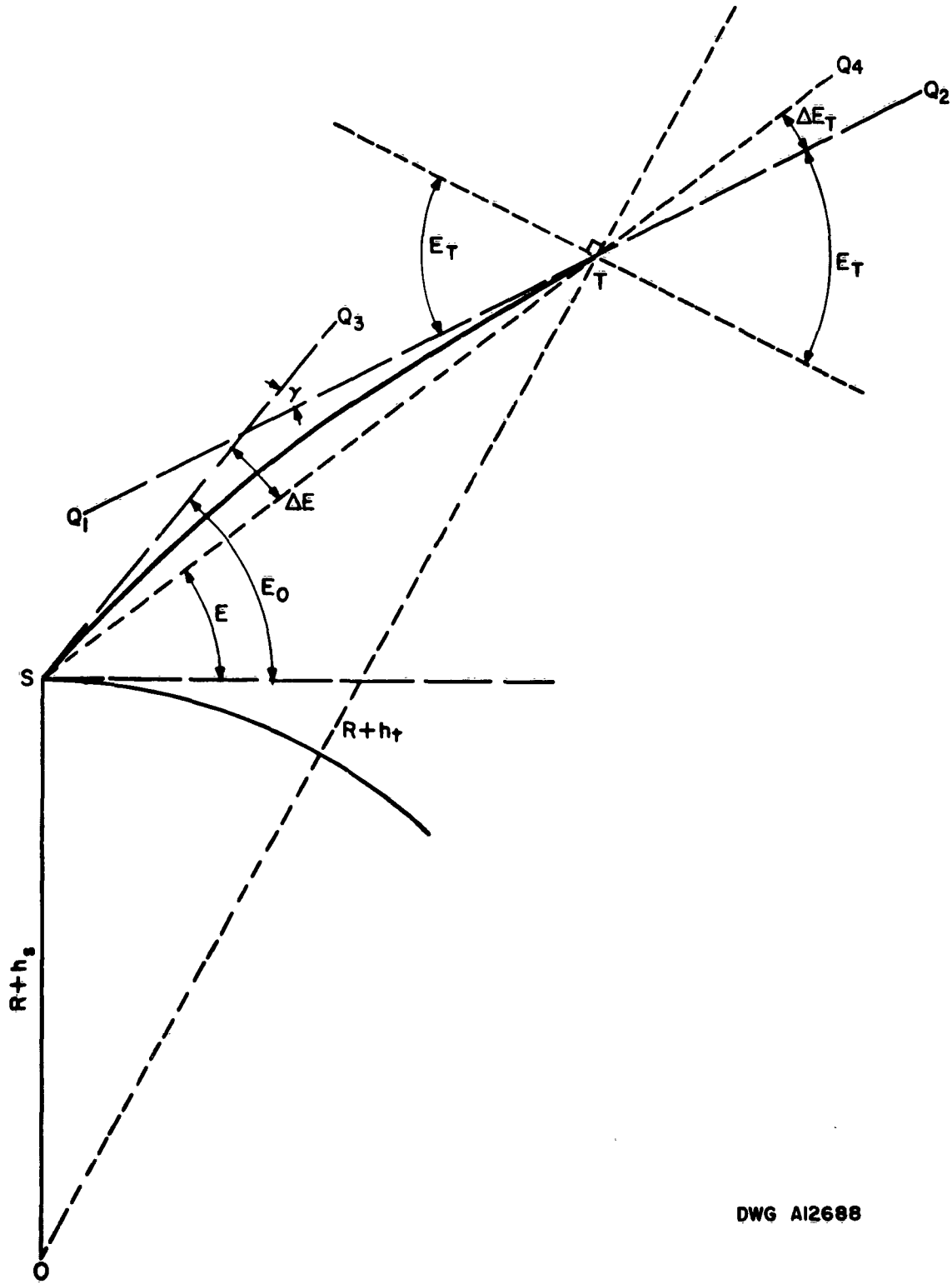

Fig. 4-1 Ray Refraction Geometry for Spherical Earth

4.4 TOTAL BENDING AND ELEVATION ANGLE CORRECTION

A method is now presented for computing the bending of radio rays, γ, through an atmosphere of "known" refractive index distribution, under the usual assumption that surfaces of equal index are spherical and concentric with the earth.

Consider a ray entering an infinitesimal layer of thickness dh at an angle β (Fig. 4-2). If K is the radius of curvature of the refracting ray, then (Ref. 12):

$$\frac{1}{K} = \frac{1}{n}\frac{dn}{dh}\cos\beta \tag{4-1}$$

where n is the index of refraction. The length of the ray path in the layer is

$$K\,d\gamma = \csc\beta\,dh. \tag{4-2}$$

This may be seen by considering the arc of a circle and two tangents intersecting each other in an angle $d\gamma$. The angle formed at the center of curvature by the two radii must also be $d\gamma$ since all angles must total 2π. The length of the enclosed arc is then $K\,d\gamma$.

If the layer is thin, the arcs may be approximated by the tangent lines; and the triangle with a hypotenuse of length dh csc β is formed. The hypotenuse length is very nearly the same as the length of the enclosed arc. Therefore, equation (4-2) is established.

$$d\gamma = \frac{1}{n}\frac{dn}{dh}\cot\beta\,dh \tag{4-3}$$

The $d\gamma$'s of all elementary layers are directly additive, as shown in Fig. 4-2. It follows, therefore, that the contribution to the total bending, γ, due to a layer bounded by the heights h_k and h_{k+1} is

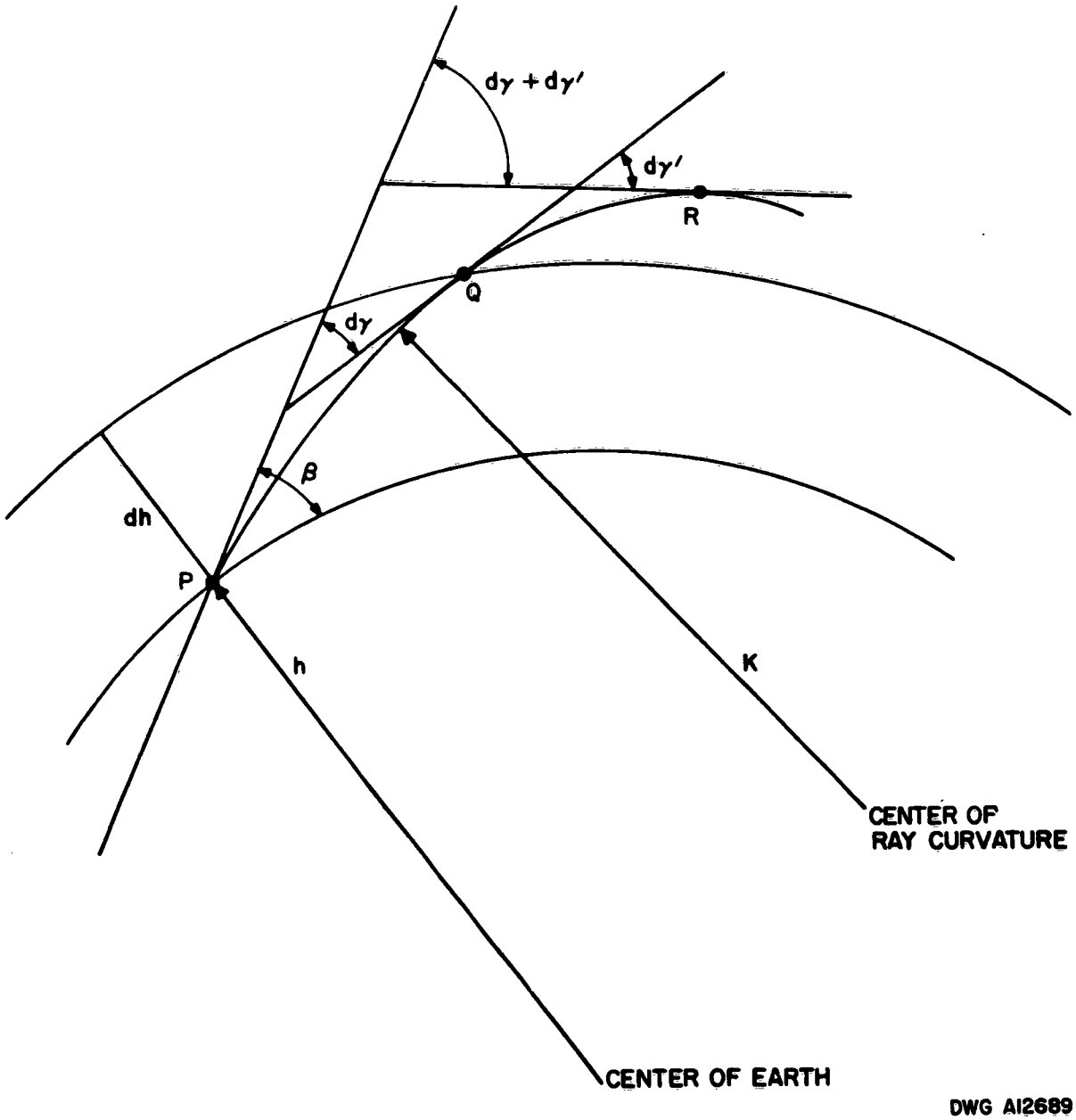

Fig. 4-2 Geometry of Bending Angle

$$\gamma_{k,k+1} = \int_{h_k}^{h_{k+1}} \frac{1}{n} \frac{dn}{dh} \cot \beta_k \, dh \, . \qquad (4\text{-}4)$$

A convenient representation for the angle β_k is now required. If the ray departs from the earth's surface at the elevation angel E_o, Bouguer's Law for spherical stratification states:

$$n_s(R + h_s) \sin (90 - E_o) = n_k(R + h_k) \sin (90 - \beta_k) = \text{constant}$$

$$n_s(R + h_s) \cos E_o = n_k(R + h_k) \cos \beta_k$$

$$\cos \beta_k = \frac{\cos E_o}{\frac{n_k}{n_s}\left[\frac{R + h_k}{R + h_s}\right]} = \frac{\cos E_o}{\left[1 - N(h_s) - N(h_k) \quad 10^{-6}\right]\left[\frac{R + h_k}{R + h_s}\right]} . \qquad (4\text{-}5)$$

Having the angle β_k, the integral equation (4-4) can be evaluated. Weisbrod and Anderson (Ref. 12) have shown that the integral has the following value for each interval h_k to h_{k+1}:

$$\gamma_{k,k+1} = \frac{|N(h_{k+1})| - |N(h_k)|}{500 \, (\tan \beta_{k+1} + \tan \beta_k)} . \qquad (4\text{-}6)$$

When these small bending angles are summed, the total bending angle is obtained:

$$\gamma = \sum_{k=0}^{j-1} \frac{|N(h_{k+1})| - |N(h_k)|}{500 \, (\tan \beta_{k+1} + \tan \beta_k)} . \qquad (4\text{-}7)$$

The total ray bending in a spherically-stratified atmosphere can be evaluated by approximating the refractivity profile by a series of straight-line segments, computing the bending due to each of the corresponding spherical shells, and adding the results to obtain the total bending.

The first step is to select a series of significant altitudes h_0, h_1, h_2, h_3, ... h_j ($h_o = h_s$, altitude of station; $h_j = h_t$, altitude of target) such that between each consecutive pair the refractivity profile is well approximated by a straight line. Usually, a number of height levels between 50 and 60 will suffice* for the total atmospheric height encountered in missile and satellite work. This will yeild sufficient accuracy while retaining the characteristics of the relatively finer structure of the atmosphere.

The next step is to tabulate the refractivity and calculate the angles β_k as in equation (4-5), then to use this information to calculate the total bending angle γ. It is known that:

$$\gamma = \Delta E_T + \Delta E.$$

Having already obtained a solution for γ, solution for ΔE_T will give an answer for ΔE. Referring again to Fig. 4-1, the law of a sines gives:

$$\frac{R + h_t}{\cos (E_o - \Delta E)} = \frac{R + h_s}{\cos (E_T + \Delta E_T)}$$

---

* The effect of varying the height increment used for refraction-correction calculations is discussed in Section 6.

or

$$E_T + \Delta E_T = \text{arc cos} \left[\frac{R + h_s}{R + h_t} \cos (E_o - \Delta E) \right]. \qquad (4\text{-}8)$$

By Bouguer's Law,

$$(R + h_t)\, n_t \cos E_T = (R + h_s)\, n_s \cos E_o,$$

or

$$E_T = \text{arc cos} \left[\frac{n_s}{n_t} \frac{R + h_s}{R + h_t} \cos E_o \right]. \qquad (4\text{-}9)$$

Hence, combining equations (4-8) and (4-9):

$$\Delta E_T = \text{arc cos} \left[\frac{R + h_s}{R + h_t} \cos (E_o - \Delta E) \right] - \text{arc cos} \left[\frac{n_s}{n_t} \frac{R + h_s}{R + h_t} \cos E_o \right]. \qquad (4\text{-}10)$$

Expanding the trigonometric functions of this expression by series and including seventh-power terms in the cosines, as is necessary to retain required accuracy:

$$- \Delta E_T \simeq \sum_{j-1}^{4} C_j \left[\frac{R + h_s}{R + h_t} \frac{n_s}{n_t} \cos E_o \right]^{2j-1} \left[\left(\frac{n_t}{n_s} \right)^{2j-1} \left(\frac{\cos (E_o - \Delta E)}{\cos E_o} \right)^{2j-1} - 1 \right]$$

or

$$- \Delta E_T \simeq \sum_{j=1}^{4} \left[\frac{R + h_s}{R + h_t} \frac{n_s}{n_t} \cos E_o \right]^{2j-1} \left[\left(\frac{n_t}{n_s} \right)^{2j-1} (1 + \Delta E \tan E_o)^{2j-1} - 1 \right]. \qquad (4\text{-}11)$$

Now since

$$\left(\frac{n_t}{n_s}\right)^{2j-1} \simeq \left[1 + \left[N(h_t) - N(h_s)\right] 10^{-6}\right]^{2j-1} \simeq 1 + (2j-1)\left[N(h_t) - N(h_s)\right] 10^{-6} \quad (4\text{-}12)$$

and

$$(1 + \Delta E \tan E_o)^{2j-1} \simeq 1 + (2j-1)\, \Delta E \tan E_o, \quad (4\text{-}13)$$

combining equations (4-12) and (4-13) results in

$$\left(\frac{n_t}{n_s}\right)^{2j-1} (1 + \Delta E \tan E_o)^{2j-1} \simeq 1 + (2j-1)\left[\left[N(h_t) - N(h_s)\right] 10^{-6} + \Delta E \tan E_o\right]. \quad (4\text{-}14)$$

Equation (4-12) for ΔE_T thus becomes:

$$-\Delta E_T \simeq \left[\left[N(h_t) - N(h_s)\right] 10^{-6} + \Delta E \tan E_o\right] \sum_{j=1}^{4} C_j (2j-1) \left[\frac{R + h_s}{R + h_t} \frac{n_s}{n_t} \cos E_o\right]^{2j-1}. \quad (4\text{-}15)$$

Since $\Delta E = \gamma - \Delta E_T$, substitution of the last equation yields:

$$\Delta E = \frac{\gamma + \left[N(h_t) - N(h_s)\right] 10^{-6} \sum_{j=1}^{4} C_j (2j-1) \left[\frac{R + h_s}{R + h_t} \frac{n_s}{n_t} \cos E_o\right]^{2j-1}}{1 - \tan E_o \sum_{j=1}^{4} C_j (2j-1) \left[\frac{R + h_s}{R + h_t} \frac{n_s}{n_t} \cos E_o\right]^{2j-1}}. \quad (4\text{-}16)$$

Furthermore:

$$\sum_{j=1}^{4} C_j(2j-1) \left[\frac{n_s}{n_t} \frac{R + h_s}{R + h_t} \cos E_o\right]^{2j-1} \simeq$$

$$\sum_{j=1}^{4} C_j(2j-1) \left[1 + (2j-1) \left[N(h_s) - N(h_t)\right] 10^{-6}\right] \left[\frac{R + h_s}{R + h_t} \cos E_o\right]^{2j-1}$$

Thus equation (4-16) becomes:

$$\Delta E \simeq \frac{\gamma + \left[N(h_t) - N(h_s)\right] 10^{-6} Y_1}{1 - \tan E_o Y_2} \qquad (4\text{-}17)$$

where

$$Y_1 = \sum_{j=1}^{4} C_j(2j-1) X^{2j-1}$$

$$Y_2 = Y_1 + \left[N(h_s) - N(h_t)\right] 10^{-6} \sum_{j=1}^{4} C_j(2j-1)^2 X^{2j-1}$$

$$X = \frac{R + h_s}{R + h_t} \cos E_o$$

$$C_1 = 1,\ C_2 = 1/6,\ C_3 = 3/40,\ C_4 = 5/112$$

By using the above equations, it is possible to reconstruct any ray path and to obtain a correction, ΔE, for the refracted elevation angle.

SECTION 5

DOPPLER CORRECTIONS

5.1 ELEVATION ANGLE REFRACTION ERROR

Let T represent a satellite transmitter location and V_p the magnitude of its velocity projected onto the plane determined by the ray path. The magnitudes of the components of the satellite velocity in the various directions shown in Fig. 5-1 are

$$\text{measured radial velocity} = V_r = V_p \cos(\psi + \Delta E_T) \tag{5-1}$$

$$\text{true radial velocity} = V_d = V_p \cos\psi \tag{5-2}$$

$$\text{apparent radial velocity} = V_a = V_p \cos(\psi - \Delta E) \tag{5-3}$$

The quantity of interest is the error in the true velocity component. The error is the difference between the true velocity component and the measured velocity component:

$$\Delta V_d = V_d - V_r. \tag{5-4}$$

Substituting values from equations (5-1), and (5-2) into equation (5-4) gives:

$$\begin{aligned}\Delta V_d &= V_p \cos\psi - V_p \cos(\psi + \Delta E_T) \\ &= V_p \cos\psi - V_p \cos\psi \cos\Delta E_T + V_p \sin\psi \sin\Delta E_T \\ &= V_p \cos\psi (1 - \cos\Delta E_T) + V_p \sin\psi \sin\Delta E_T. \end{aligned} \tag{5-5}$$

Since ΔE_T is a very small angle, the trigonometric functions can be expanded by series to the second order:

$$\Delta V_d \simeq V_p \left[\Delta E_T \sin\psi + \tfrac{1}{2}(\Delta E_T)^2 \cos\psi\right]. \tag{5-6}$$

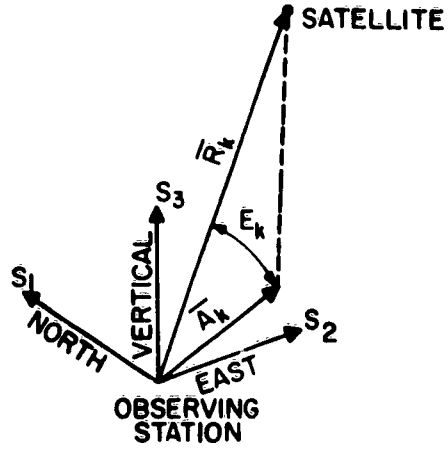

STATION COORDINATE SYSTEM

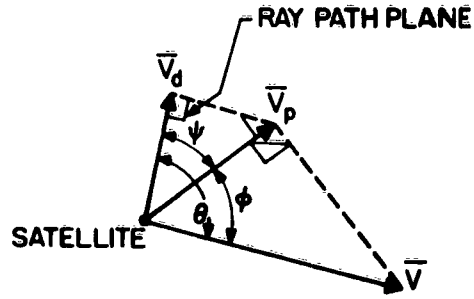

CONFIGURATION OF VELOCITY VECTORS AT THE SATELLITE

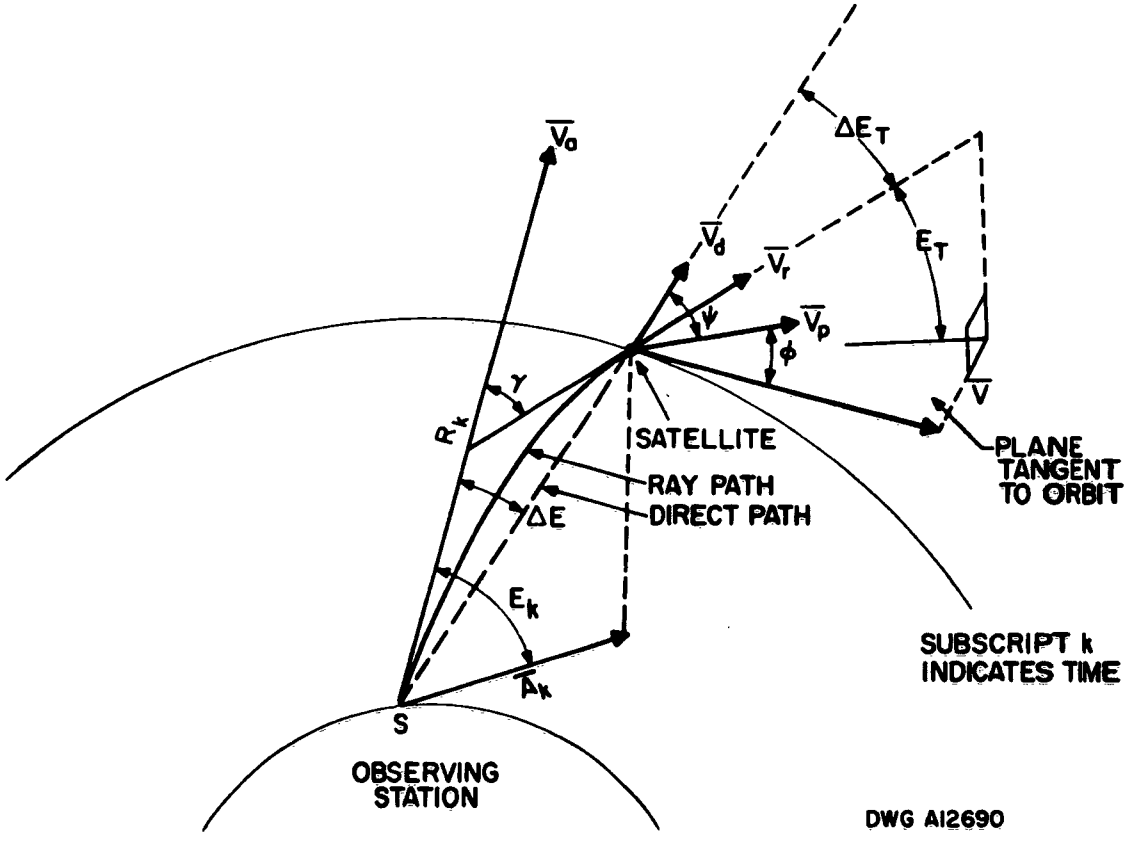

Fig. 5-1 Geometry for Doppler Refraction Error Analysis

For cases where ψ is reasonably different from zero, this expression may be reduced to

$$\Delta V_d \cong V_p \, \Delta E_T \sin \psi. \tag{5-7}$$

5.2 ONE-WAY DOPPLER REFRACTION ERROR

From Section 2, the one-way Doppler frequency shift is

$$f_d = \frac{f_o}{c} n_t \frac{ds}{dt}.$$

The time rate of change of the signal path length is ds/dt. This signal path length is not too different from the slant range, R; therefore, the time rate of change of both s and R should not be appreciably different and could be approximated as

$$\frac{ds}{dt} \cong \frac{dR}{dt} = \dot{R}.$$

By also substituting $\dot{R} = V \cos \theta$, where θ is the angle between the true velocity, V, and the position vector of the satellite relative to the station, the resulting formula for one-way Doppler frequency shift becomes

$$\begin{aligned} f_d &= (f_o/c)\, n_t\, V \cos \theta \\ &= (f_o/c)\, n_t\, V_d \\ &= (f_o/c)\, n_t\, V_p \cos \psi \\ &= (f_o/c)\, n_t\, V \cos \theta \cos \psi \end{aligned} \tag{5-8}$$

where θ = angle between V and the ray path plane,

f_d = Doppler shift, or difference between the transmitted frequency and the apparent received frequency,

f_o = transmitted frequency,

c = velocity of light in a vacuum, and

n_t = index of refraction at the target location corresponding to the transmitted frequency f_o.

Differentiating equation (5-8), the error in Doppler frequency due to the velocity error is

$$\Delta f_d = (f_o/c)\, n_t \cos \psi\, \Delta V_p \qquad (5\text{-}9)$$

where f_o, c, n_t, and ψ are assumed to be errorless quantities.

By differentiating equation (5-2), the resulting expression is

$$\Delta V_d = \Delta V_p \cos \psi$$

Equation (5-9) becomes

$$\Delta f_d = (f_o/c)\, n_t\, \Delta V_d$$

which, when combined with equation (5-6), yields:

$$\Delta f_d = (f_o/c)\, n_t\, \Delta V_d = (f_o/c)\, n_t\, V_p\left[\Delta E_T \sin \psi + \tfrac{1}{2}(\Delta E_T)^2 \cos \psi\right]. \qquad (5\text{-}10)$$

Calculation of the angle ΔE_T has been discussed in Section 4. With this result, it is possible to calculate the Doppler frequency error due to refraction in the case of one-way Doppler transmission.

5.3 TWO-WAY DOPPLER REFRACTION ERROR

Using the two-way Doppler expression, equation (2-6), the Doppler frequency error due to refraction in two-way transmission is

$$\Delta f_{dg} = \left[(a + bf_o)n_t + n_s bf_o\right] V_p \left(\Delta E_T \sin \psi + \frac{1}{2} \Delta E_T^2 \cos \psi\right). \quad (5\text{-}11)$$

5.4 DOPPLER ERROR CORRECTION EXPRESSIONS

The computation of errors induced by refraction of doppler transmissions, as developed in previous sections, requires a method for calculating the angle ψ. With reference to Fig. 5-1, construct the station centered, left-handed Cartesian coordinate system (S_1, S_2, S_3) and corresponding unit vectors ($\bar{S}_1$, $\bar{S}_2$, $\bar{S}_3$) respectively, where the S_1 axis is directed toward true north, the S_2 axis east, and the S_3 axis vertical so that the vector $\bar{S}_3$ points along the vertical axis and is given by the vector product $\bar{S}_3 = \bar{S}_2 \otimes \bar{S}_1$.

For any given satellite pass at time t_k, the following observed parameters are defined as:

R_k = slant range (range from station to vehicle),

A_k = azimuth angle (measured from true north), and

E_k = elevation angle (measured from the (S_1, S_2) plane).

The position vector, $\bar{P}_k$, from the station to the vehicle at time t_k is expressed as:

$$P_k = (R_k \cos A_k \cos E_k)\, \bar{S}_1 + (R_k \sin A_k \cos E_k)\, \bar{S}_2 + (R_k \sin E_k)\, \bar{S}_3. \quad (5\text{-}12)$$

Furthermore, the azimuth vector, $\bar{A}_k$, the normalized projection of vector $\bar{P}_k$ on the (S_1, S_2) plane, is defined as:

$$\bar{A}_k = (\cos A_k)\, \bar{S}_1 + (\sin A_k)\, \bar{S}_2. \quad (5\text{-}13)$$

The curved ray path, S, of the doppler transmission is taken to be in the plane formed by the vectors $\bar{P}_k$ and $\bar{A}_k$, so that the vector $\bar{N}_k$, a unit normal vector to this plane, is given as:

$$\bar{N}_k = \frac{1}{R_k \sin E_k} (\bar{P}_k \otimes \bar{A}_k), \text{ since } (\bar{P}_k \otimes \bar{A}_k) = R_k \sin E_k \quad (5\text{-}14)$$

or

$$\bar{N}_k = (\sin A_k)\, \bar{S}_1 - (\cos A_k)\, \bar{S}_2. \quad (5\text{-}15)$$

The vehicle velocity vector, $\bar{V}_k$, is expressed by a finite vector difference between two consecutive position vectors as:

$$\bar{V}_k = \frac{(\bar{P}_{k+1} - \bar{P}_k)}{(t_{k+1} - t_k)} \quad (5\text{-}16)$$

The component of the velocity vector, $\bar{V}_k$, in the ray path plane is represented by the vector $\bar{V}_p$, which is formed by the vector product of $\bar{V}_k$ and $\bar{N}_k$ so that:

$$\bar{V}_p = \bar{V}_k \otimes \bar{N}_p. \quad (5\text{-}17)$$

The angle ψ is defined as the angle between the vector $\bar{V}_p$ and the vector $\bar{V}_d$. The vector $\bar{V}_d$ is defined as the true (errorless) station-to-vehicle velocity vector. $\bar{V}_d$ lies in the ray path plane since refraction errors affect only elevation angles. The angle ψ is expressed as:

$$\psi = \arccos \left[\frac{\bar{V}_p \quad \bar{V}_d}{|V_p|\ |V_d|} \right]. \quad (5\text{-}18)$$

However, in the normal case of data reduction, data is not available for the vector $\bar{V}_d$. The vector $\bar{V}_d$ can be approximated (in direction, only) by normalizing the vector $\bar{P}_k$ corrected for elevation errors due to refraction. (Approximate values for the elevation errors, ΔE, are found in Fig. 5-6.)

Denote the corrected vector $\bar{P}_k$, which is normalized to magnitude one, as the vector $\bar{\rho}_k$ so that,

$$\bar{\rho}_k = \left[\cos A_k \cos (E_k + \Delta E_k)\right] \bar{S}_1 + \left[\sin A_k \cos (E_k + \Delta E_k)\right] \bar{S}_2 + \sin (E_k + \Delta E_k)\, \bar{S}_3. \tag{5-19}$$

Then the angle ψ is expressed as:

$$\psi = \cos^{-1}\left[\frac{\bar{V}_p \cdot \bar{\rho}_k}{|V_p|}\right]. \tag{5-20}$$

5.5 ORBITAL VELOCITY ERROR

The magnitude of the error induced in orbital velocity due to refraction effects is denoted by ΔV.

The values of the angle ψ, obtained from equations (5-10) and (5-11), determine the results for Δf_d, so that ΔV_d is given by $\Delta V_d = \lambda \Delta f_d$, where λ is the wave length corresponding to f_o.

From equation (5-2) and the geometry in Fig. 5-1, the errors in magnitude of vectors $\bar{V}_p$ and $\bar{V}$ are given as

$$\Delta V_p \approx \Delta V_d \sec \psi \tag{5-21}$$

$$\Delta V \approx \Delta V_p \sec \phi \tag{5-22}$$

where ϕ is the angle between $\bar{V}$ and $\bar{V}_p$ and is given by:

$$\phi = \cos^{-1}\left[\frac{|\bar{V}_p|}{|V|}\right] \tag{5-23}$$

Combining the above results, the error in orbital velocity becomes

$$\Delta V = \frac{|\bar{V}_p|}{|V|} \lambda \Delta f_d . \tag{5-24}$$

Figure 5-2 and Table 5-1 give examples of results of accuracy expected for Doppler errors based on the development of the above and previous analyses.

5.6 REFRACTION CORRECTION FOR ORBITAL ERROR

In determining the correction for refraction effects, let

$f_{do}(t)$ = observed one-way Doppler frequency shift at time t,

$E_o(t)$ = observed elevation angle at time t,

$f_d(t)$ = Doppler frequency shift at time t in absence of atmosphere,

$E(t)$ = elevation angle at time t in absence of atmosphere, and

ΔE = refraction error in apparent elevation angle E_o at time t.

It is obvious that:

$$E_o(t) = E(t) + \Delta E.$$

If the refraction error is

$$\Delta E = \frac{dE}{dt} \Delta T = E'(t)\Delta t,$$

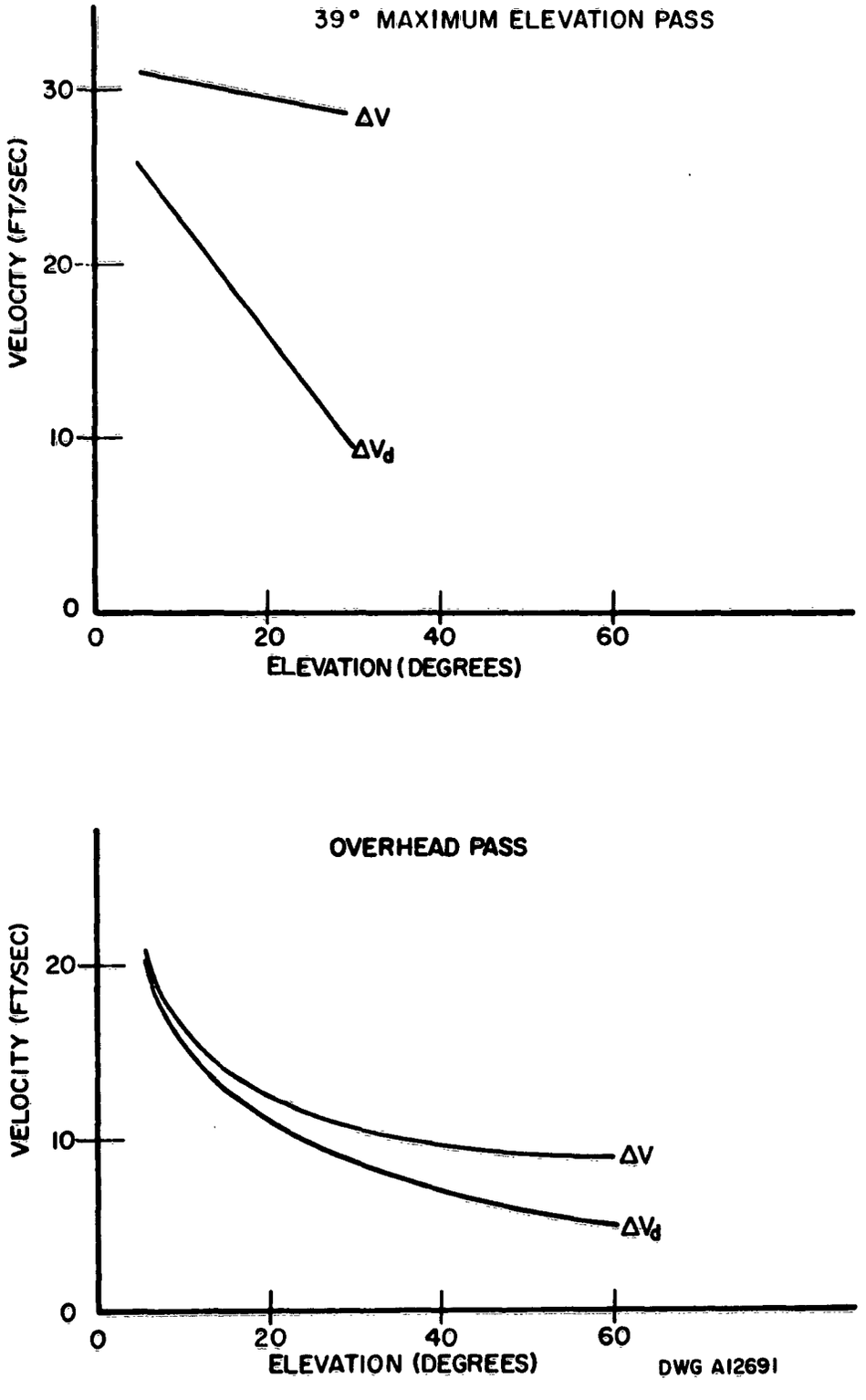

Fig. 5-2 Velocity Errors Induced by Doppler Refraction Effects

TABLE 5-1

DOPPLER PROPAGATION EFFECTS
FOR 400 MC TRANSMISSION FROM 125 N.M. CIRCULAR ORBIT

PARAMETER	OVERHEAD PASS				MAX. $E_o = 39^\circ$ PASS	
	ELEVATION				ELEVATION	
	5°	30°	45°	60°	5°	30°
γ = Total Bending Angle	6.9 mils	1.2 mils	0.7 mils	0.4 mils	6.9 mils	1.2 mils
ΔE = Elevation Angle Error	2.5 mils	0.6 mils	0.3 mils	0.18 mils	2.5 mils	0.6 mils
$\Delta E_T = \gamma - \Delta E$	4.4 mils	0.6 mils	0.4 mils	0.22 mils	4.4 mils	0.6 mils
ψ = Angle between vectors $\bar{V}_p$ and $\bar{V}_d$	10.5°	26.5°	43.0°	53.4°	70°	60°
f_o = Doppler Frequency Error due to refraction	8.1 cps	3.2 cps	2.8 cps	1.87 cps	10.3 cps	3.83 cps
ΔV_D = Corresponding Error in Relative Velocity	20.2 fps	8.0 fps	7.1 fps	4.7 fps	25.7 fps	9.6 fps
ΔV = Corresponding Error in Orbital Velocity	20.6 fps	9.0 fps	9.8 fps	7.9 fps	31.1 fps	28.6 fps

then

$$E_o(t) = E(t) + E'(t)\Delta t = E(t + \Delta t)$$

or, equivalently:

$$E(t) = E_o(t - \Delta t) = E_o(t) - E_o'(t)\Delta t,$$

where

$$\Delta t = \frac{|\Delta E|}{E_o'(t)}. \qquad (5\text{-}25)$$

Equation (5-25) shows how to recalibrate the time scale so that the true (vacuum) value of the elevation angle, E, may be expressed as the value of the observed elevation, E_o, at some other time. It follows that the same transformation of the time scale will give the true value of the Doppler shift, f_d, in terms of the observed Doppler shift, f_{do}, at the transformed time value:

$$f_d(t) = f_{do}(t - \Delta t). \qquad (5\text{-}26)$$

Figure 5-3 shows the application of this method. The observed values f_{do} and E_o are represented by solid curves, while f_d and E are represented by dashed lines.

The corrected elevation curve was obtained from the refraction formulas, equations (4-5) and (4-7). The corrected Doppler shift curve was plotted by taking time shifts (Δt) corresponding to the time difference between the two elevation curves. This same time difference, when applied to the observed Doppler curve, forms the corrected frequency shift curve shown in Fig. 5-3.

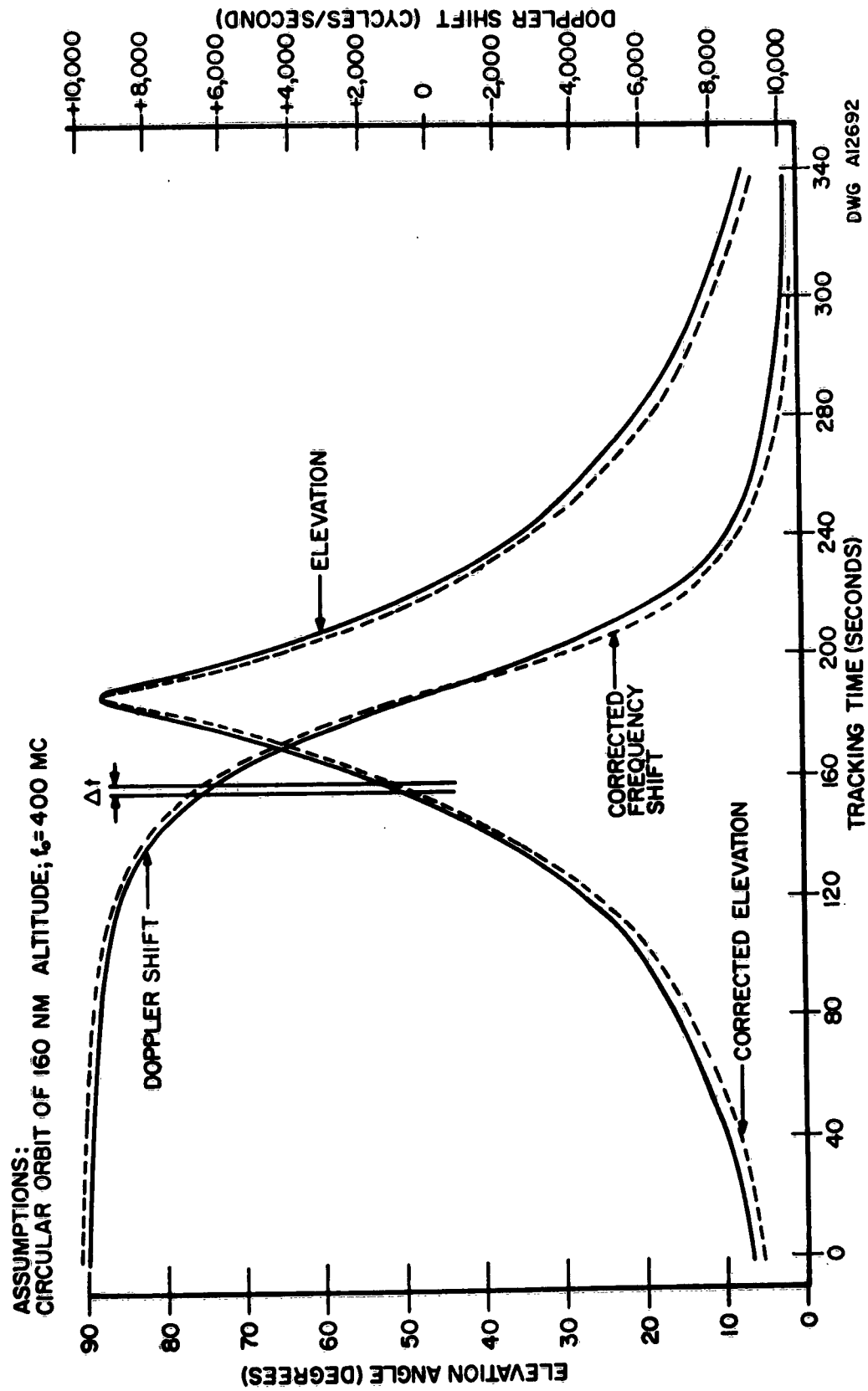

Fig. 5-3 Time Scale Correlation for Doppler Orbital Curve

SECTION 6

EXPECTED ACCURACY OF DOPPLER MEASUREMENTS

6.1 GENERAL

Determination of accuracies in any refraction correction procedure is considered one of the important aspects of the present study. Computations were carried out (Ref. 3) to demonstrate the effects of the size of increments in the expression used to approximate typical refraction-correction integrals. Similar calculations were made to illustrate the effect of rather drastic approximations to the shape of ionospheric layers as well as to determine the effect of changing the height of such layers. Based upon these results, an analysis using results of numerical work by Counter and Reidel (Ref. 5) was conducted to estimate accuracies expected of refraction-correction procedures. A determination of the errors resulting from uncertainty in the local index at the target was the basis of another analysis.

6.2 EFFECT OF INCREMENTAL ALTITUDE CALCULATIONS

In obtaining the correction, ΔE, to the apparent elevation angle, E_o, the total bending, γ, must be calculated through use of a finite-summation approximation to an integral. Often the values of h_k in this expression are conveniently chosen to be equally spaced with a certain altitude increment. For example, Weisbrod and Anderson (Ref. 12) state that the resultant error in tropospheric bending is only about 9.6 percent for a 10-mile increment.

An analysis was conducted (Ref. 3) to check the effect of selected increments upon ionospheric refraction corrections. The results of these calculations indicate that the increment chosen for calculation has a smaller effect upon the results than might be expected at first. However, wherever reasonably high accuracies are required in the correction procedures, smaller increments should be used to preserve the details of the refractivity profile, assuming the profile itself is sufficiently well known to warrant this procedure.

6.3 CHAPMAN MODEL LINEAR APPROXIMATION ERRORS

The effect of ionospheric layer shape was investigated (Ref. 3) by approximating the refractivity profile corresponding to the 97.5 percentile curve of Fig. 3-3 by a relatively small number of straight-line segments (in this case, five). The approximate profile thus obtained was compared to the original profile in Fig. 6-1. The linear approximation to the refractivity profile is given by the following function (for 400 Mc):

Altitude (n.m.)	Approximate Refractivity (N units)	
$150 < h \leq 600$	$-1550 \exp(-.0096\, h)$	$= N(h)$
$97 < h \leq 150$	$-71 \exp(+.011\, h)$	
$76 < h \leq 97$	$-.027 \exp(+0.092\, h)$	
$53 < h \leq 76$	$-601 \exp(-.039\, h)$	
$45 \leq h \leq 53$	$-45 \times 10^{-8} \exp(+0.37\, h)$	

In a previous experiment (Ref. 3), it was observed that ΔE calculated from the true profile differed from ΔE calculated from the linear approximation by less than 0.05 mr in most cases. The linear approximation is sufficiently accurate, therefore, to use in the calculation of bending and elevation angle error.

6.4 EFFECT OF IONOSPHERIC LAYER HEIGHT CHANGES

The effect of changes in the height of the maximum chosen for the F-layer of the ionosphere was investigated (Ref. 3) for $f_o = 100$ Mc by using the linear approximation profile for comparison purposes. The F-layer portion of this profile was moved up in height by 10 and 25 n.m., and the resulting elevation angle errors were calculated.

It was concluded that the choice of the height of the ionspheric layer has a most important effect upon the values attained for refraction corrections.

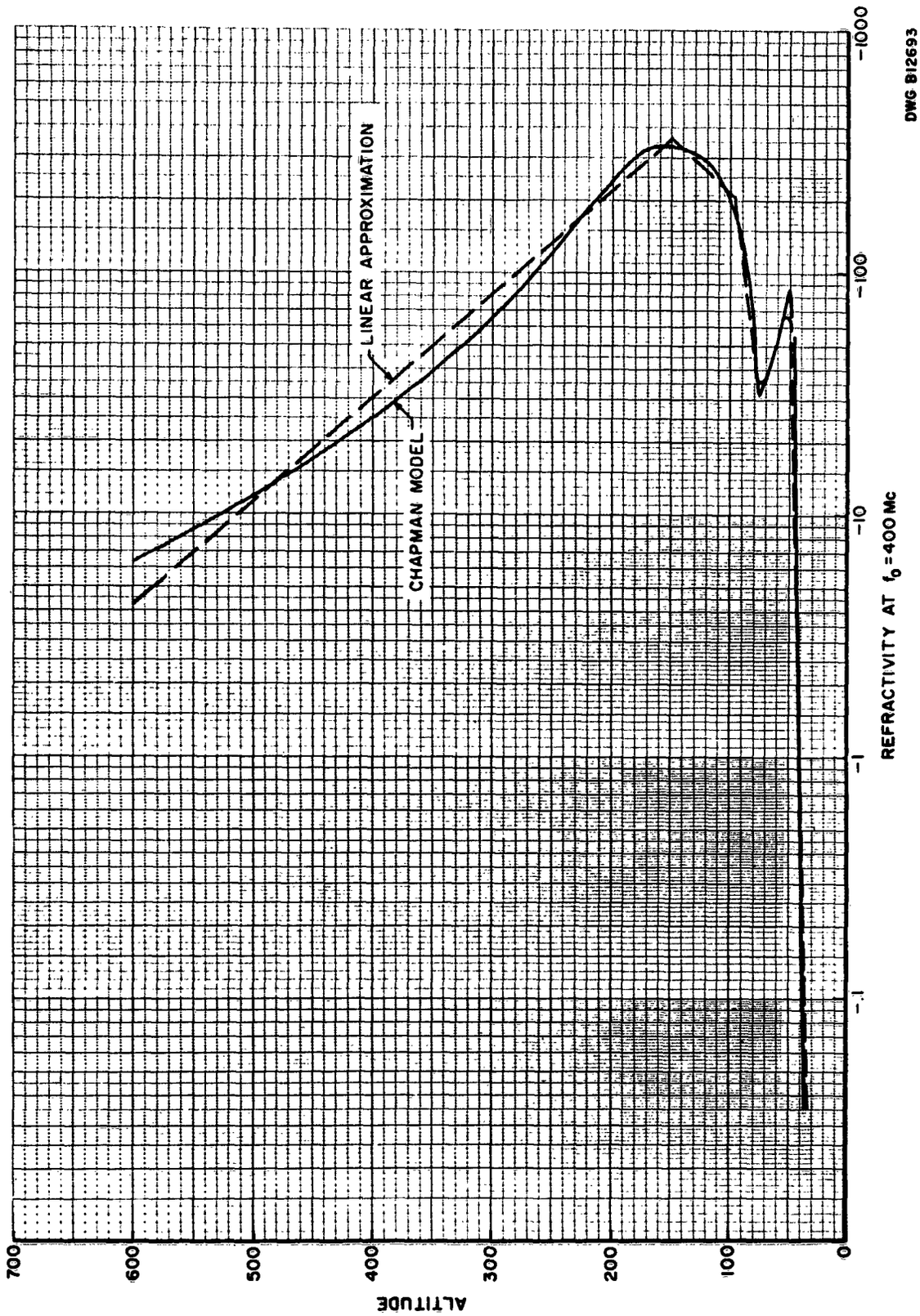

Fig. 6-1 Linear Approximation to the Chapman Model

6.5 EFFECT OF ANGULAR ERROR STANDARD CORRECTIONS

In addition to the foregoing analyses, expected accuracies of standard corrections were investigated with the aid of numerical work by Counter and Riedel (Ref. 5). For example, Figs. 6-2 through 6-5 summarize the results of a standard refraction correction applied in a case where f_o = 400 Mc. The graphs show the expected value of the elevation angle deviation, $E_o - E$, the standard correction, ΔE, applied, and the standard deviation of the bias remaining in the elevation angle, with and without the application of a correction based on a measured value of the index of refraction at the ground at the time of the observation of the target. All of the curves are drawn as contours of constant, true elevation angle, E.

The fact that the curves in Figs. 6-4 and 6-5 are not all zero for an arbitrary altitude indicates the failure of the standard atmosphere to conform precisely to the actual atmosphere. From Fig. 6-4, it may be seen that the angular refraction corrections for the tropospheric ($h < 40$ n.m.) bias errors should have good accuracy (better than 0.05 mils) at elevation angles greater than 30 degrees. It may be concluded from Fig. 6-5 that the added knowledge of surface index of refraction should give good accuracies for elevation angles greater than 6 degrees.

For ionospheric effects on angle measurement, however, the standard correction will not give comparable results. Data from ionospheric soundings will be necessary to obtain the greater accuracies which are necessary for precise Doppler velocity measurements.

6.6 EFFECT OF DOPPLER MEASUREMENT STANDARD CORRECTIONS

Referring to equation (5-10), it can be seen that the maximum ΔE_T must be on the order of 10^{-6} mils or less if the accuracy in the velocity correction is to approach 0.01 foot per second. However, Figs. 6-4 and 6-5 show that it is doubtful whether this accuracy can be achieved under the best conditions. Even if the accuracy is relaxed to 0.1 foot per second, a standard correction for tropospheric effects will not yield

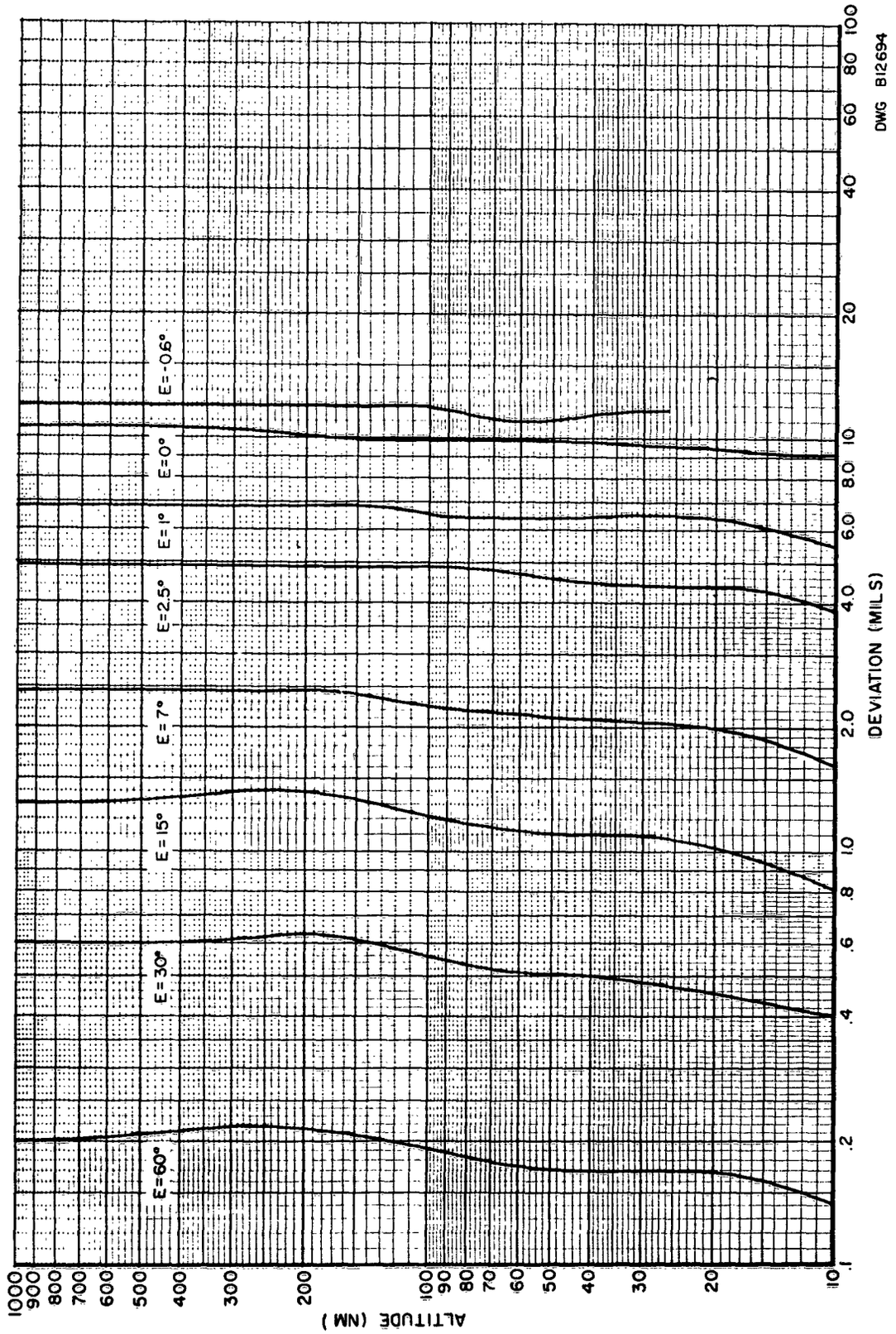

Fig. 6-2 Expected Elevation Angle Deviation

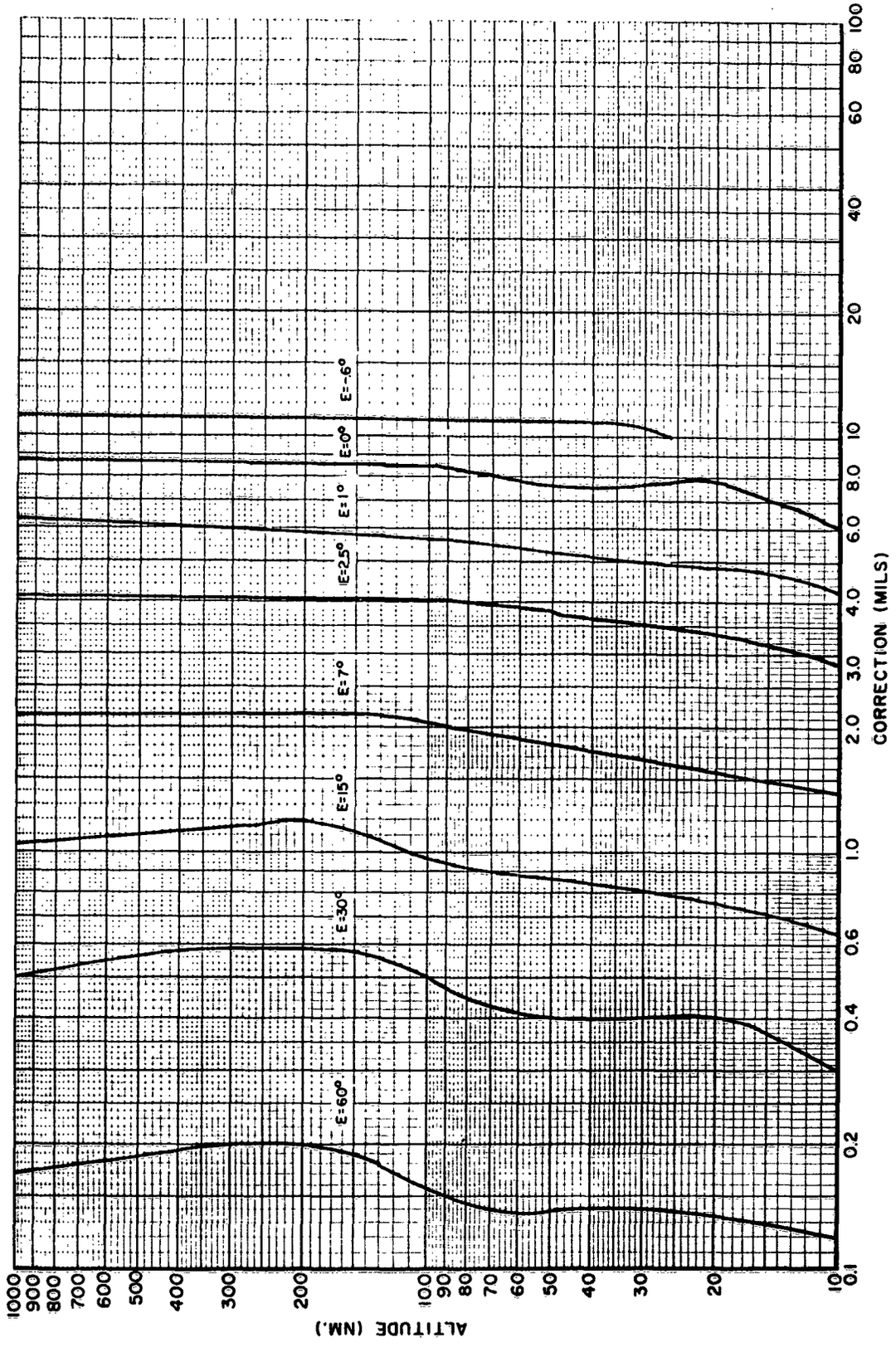

Fig. 6-3 Standard Elevation Angle Correction

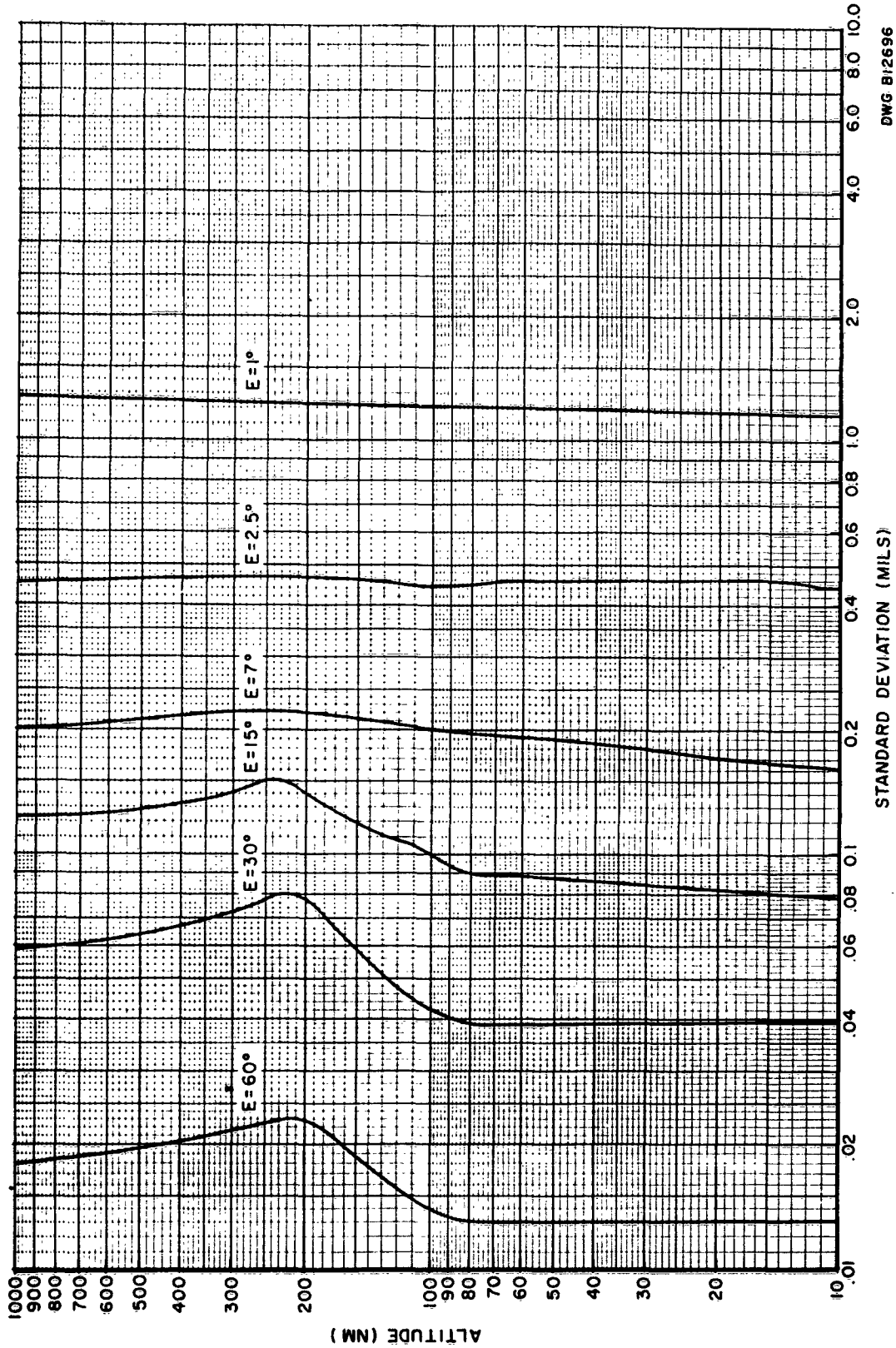

Fig. 6-4 Standard Deviation of Elevation Angle Bias

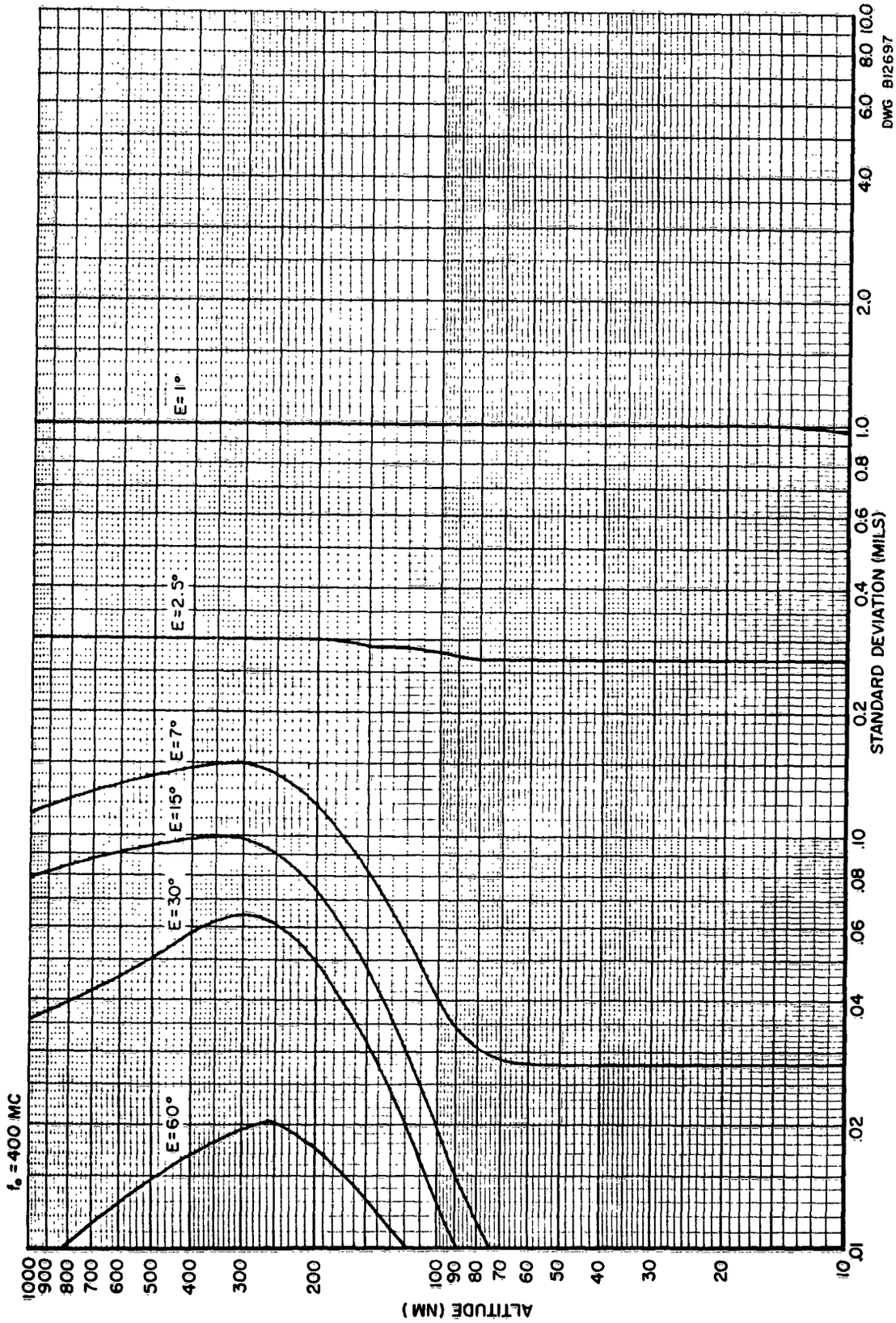

Fig. 6-5 Standard Deviation of Elevation Angle Bias Using Measured Index of Refraction at Station

the desired accuracy without measuring the local surface index or refraction. An accuracy of 0.1 foot per second is suitable (according to Ref. 3) for ionospheric predictions and other similar data, but only for angles greater than about 15 degrees.

6.7 EFFECT OF LOCAL INDEX UNCERTAINTY AT TARGET

An additional error is introduced if the effect of the local index at the target is not considered when converting from Doppler frequency to Doppler velocity. From equation (5-10), it is evident that the effect of the local index can be important in making the conversion. Assuming a target in the ionosphere transmitting to a ground station, the ionospheric index from equation (3-4) is

$$n_t = \sqrt{1 - 80.5\,(N_e/f_o^2)} \simeq 1 - 40.2\,(N_e/f_o^2) \qquad (6\text{-}1)$$

or, from equation (3-2):

$$n_t = \sqrt{1 - (f_c/f_o)^2} \simeq 1 - (1/2)(f_c/f_o)^2. \qquad (6\text{-}2)$$

Now since $\dot{R} = f_d\lambda$, where $\lambda = c/f_o n_t$,

$$\dot{R} = \frac{f_d c}{f_o n_t}. \qquad (6\text{-}3)$$

Differentiating this expression to find the dispersion corresponding to an uncertainty in knowledge of local index:

$$\Delta\dot{R} = \frac{f_d c}{f_o n_t^2}\,\Delta n_t.$$

Therefore:

$$\frac{\Delta\dot{R}}{\dot{R}} = \frac{\Delta n_t}{n_t} \cong \Delta n_t . \qquad (6\text{-}4)$$

In the ionosphere, where this effect can become important, the expressions for ionospheric index, (6-1) and (6-2), yield by differentiation:

$$-\Delta n_t = \frac{40.5}{f_o^2}\Delta N_e = \frac{f_c}{f_o^2}\Delta f_c . \qquad (6\text{-}5)$$

Combining equations (6-4) and (6-5):

$$\Delta\dot{R} = -\dot{R}\frac{f_c}{f_o^2}\Delta f_c = -\dot{R}\frac{40.5}{f_o^2}\Delta N_e . \qquad (6\text{-}6)$$

Hence, the velocity error will depend upon the uncertainty in knowledge of the critical frequency or electron density. Figure 6-6 shows these velocity errors as a function of operating frequency for different values of uncertainty in critical frequency. The maximum, mean, and minimum curves correspond to values obtained from the curves of Fig. 3-2 at an altitude of 125 n.m.

For this typical case, with an effective target velocity of 25,230 feet per second, an uncertainty in critical frequency of 1 Mc will prevent accuracies of better than 1 foot per second at operating frequencies below about 350 Mc and greater than 0.1 foot per second below about 1100 Mc. Increasing the critical frequency accuracies by a factor of 10 increases the velocity accuracy by the same factor.

Figure 6-7 is an elaboration of the information in Fig. 6-6 for the particular case of f_o = 400 Mc. Doppler velocity error is shown as a function of uncertainty in critical frequency and the maximum, mean, and minimum curves are shown.

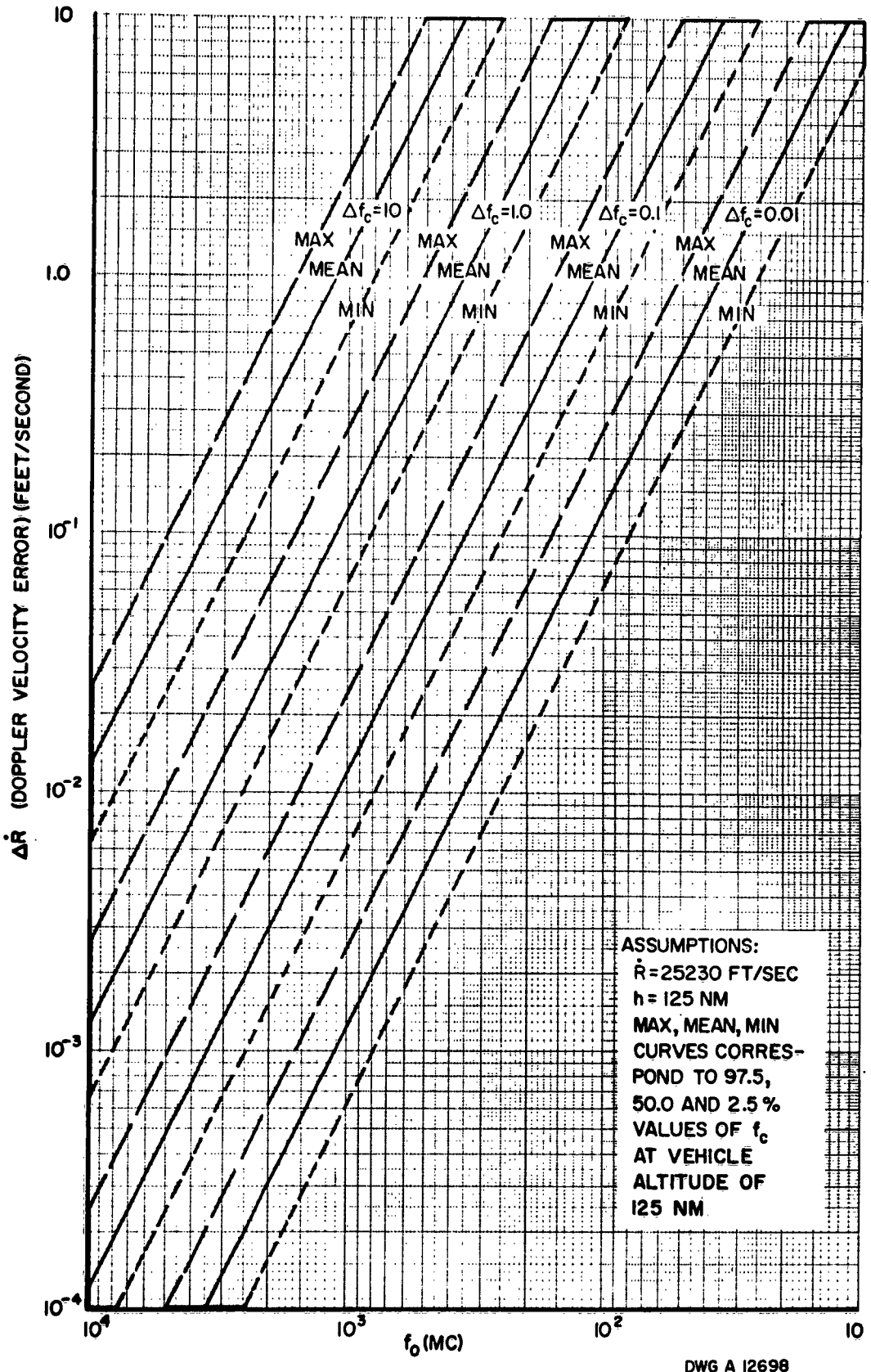

Fig. 6-6 Doppler Velocity Error vs. Operating Frequency for Selected Errors in Critical Frequency

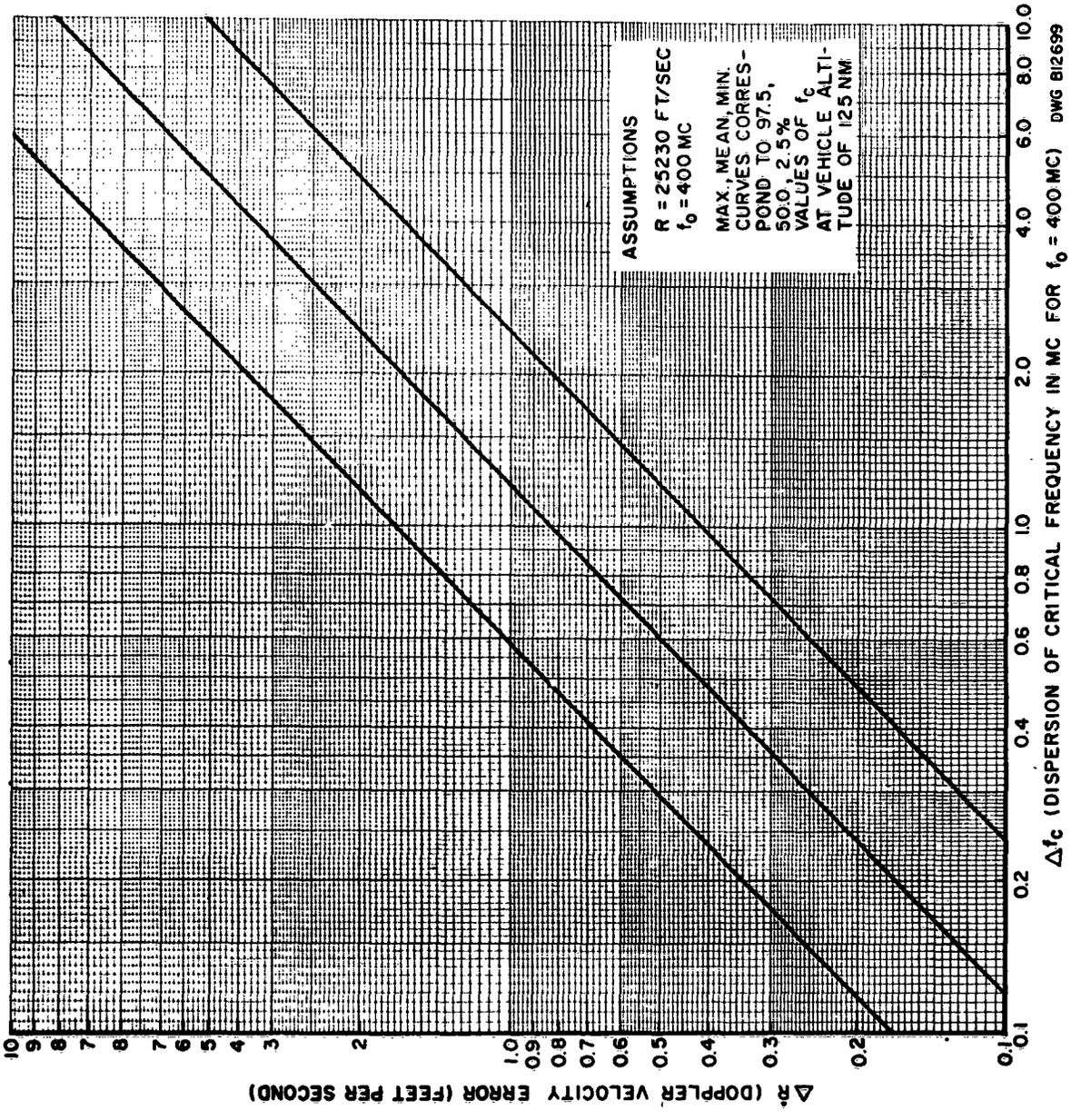

Fig. 6-7 Doppler Velocity Error vs. Errors in Critical Frequency at Operating Frequency of 400 Mc

BIBLIOGRAPHY

1. Bean, B. R.; and Thayer, G. D.; "Models of the Atmospheric Radio Refractive Index"; Proc. of IRE, Vol. 47, No. 5, May 1959, pp. 740-755.

2. Bean, B. R., and Horn, J. D.; "Radio-Refractive-Index Climate Near the Ground"; J. Res. N.B.S., Vol. 63D, No. 3, November-December 1959, pp. 259-271.

3. Berger, W. J., and Ricupito, J. R.; "Refraction Correction Studies, Final Report"; Aeronutronic Technical Report U-954, July 1960.

4. Counter, V. A.; "Propagation of Radio Waves Through the Troposhere and Ionosphere"; Lockheed Aircraft Corp. Report, LMSD 2066-R1, May 1958.

5. Counter, V. A., and Riedel, E. P.; "Calculations of Ground-Space Propagation Effects"; Lockheed Aircraft Corp. Report, LMSC 2461, May 1958

6. Dixon, H. M.; "A First Order Approximation Correction of Radar Elevation Angles for Tropospheric Refraction"; White Sands Proving Ground, New Mexico, Tech Report 18E, January 1957.

7. Guier, W. H., and Weiffenbach, G. C.; "A Satellite Doppler Navigation System"; Proc. of IRE, April 1960, pp. 507-516.

8. Millman, G. H.; "Atmospheric Effects on VHF and UHF Propagation"; Proc. of IRE, August 1958, pp. 1492-1501.

9. Monroe, A. J.; "A Doppler Primer"; Litton Industries Report, June 1957.

10. Thomas, P. D.; "Use of Artificial Satellite for Navigation and Oceanographic Surveys"; U. S. Government Printing Office, Technical Bulletin No. 12, July 1960 (U. S. Department of Commerce, Coast and Geodetic Survey).

11. Space Technology Laboratories Report GM-TM-0165-00307; "Refraction Corrections"; Los Angeles, California, 31 December 1958.

12. Weisbrod, S., and Anderson, L. J.; "Simple Method for Computing Tropospheric and Ionospheric Refractive Effects on Radio Waves"; Proc. of IRE, Vol. 47, No. 10, October 1959, pp. 1770-1777.

DISTRIBUTION LIST

Address	No. of Copies
Commander Space Systems Division Air Force Systems Command Air Force Unit Post Office Los Angeles, California Attn: Technical Data Center	10
USAF Contract Support Detachment No. 3 Philco Corporation Western Development Laboratories Palo Alto, California	1
ASTIA Arlington Hall Station Arlington 12, Virginia	10
Philco Corporation Western Development Laboratories Palo Alto, California	101 + 1 reproducible
Philco Corporation (Plant 50) 4700 Wissahickon Ave. Philadelphia 44, Pennsylvania	1
Philco Corporation (Plant 37) Union Meeting Road Blue Bell, Pennsylvania	1
Philco Computer Division 3900 Welsh Road Willow Grove, Pennsylvania	1
	125 + 1 reproducible